AN EXPERIMENTAL INVESTIGATION OF IMPACT EFFECTS ON OPEN ENDED STEEL CYLINDRICAL SHELLS

A THESIS

Presented to

The Faculty of the Graduate Division

by

Stephen Lee Passman

In Partial Fulfillment

of the Requirements for the Degree

Master of Science in Engineering Mechanics

Georgia Institute of Technology

June 1966

AN EXPERIMENTAL INVESTIGATION OF IMPACT EFFECTS

ON OPEN ENDED STEEL CYLINDRICAL SHELLS

Approved:

Date Approved by Chairman: 4-7-66

ACKNOWLEDGEMENTS

I wish to thank Dr. Charles E. Stoneking and Dr. Wilton W. King for their kind advice and encouragement, and Mr. Mike Haycock for his help in performing the experiments.

TABLE OF CONTENTS

		Page
ACKNOWLEDGMENTS		ii
LIST OF TABLES		iv
LIST OF ILLUSTRATIONS		v
SUMMARY		vii
LIST OF SYMBOLS		viii
Chapter		
I.	INTRODUCTION	1
	Purpose of the Research Definition of the Problem History and Literature Review	
II.	DIMENSIONAL ANALYSIS	5
III.	INSTRUMENTATION AND EQUIPMENT	10
	Air Gun Hopkinson Pressure Bar Photogrid Process High Speed Motion Pictures	
IV.	RESULTS	29
V.	CONCLUSIONS	55
VI.	RECOMMENDATIONS	57
APPENDIX		72
LITERATURE CITED		73

LIST OF TABLES

Table		Page
1.	Summation of Computer Print-Out.	50
2.	Failure Velocities for the Cylinders Tested as Calculated from Equation 22.	51
3.	Summary of Experimental Results.	52
4.	Data Sheet for Shot 18	69
5.	Data Sheet for Shot 45	70

LIST OF ILLUSTRATIONS

Figure		Page
1.	Floor Plan of the Impact Laboratory.	11
2.	Operation of the Air Gun	12
3.	Strain Gage Oscilloscope Trace for Shot 37	19
4.	Failure Velocity as a Function of $\frac{t}{D}$ and $\frac{L}{D}$.	31
5.	Strain Versus Nondimensional Length.	32
6.	Strain Versus Nondimensional Length.	33
7.	Strain Versus Nondimensional Length.	34
8.	Strain Versus Nondimensional Length.	35
9.	Strain Versus Nondimensional Length.	36
10.	Strain Versus Nondimensional Length.	37
11.	Strain Versus Nondimensional Length.	38
12.	Strain Versus Nondimensional Length.	39
13.	Strain Versus Nondimensional Length.	40
14.	Strain Versus Nondimensional Length.	41
15.	Strain Versus Nondimensional Length.	42
16.	Strain Versus Nondimensional Length.	43
17.	Strain Versus Nondimensional Length.	44
18.	Strain Versus Nondimensional Length.	45
19.	Strain Versus Nondimensional Length.	46
20.	Force Versus Nondimensional Velocity	47
21.	Force Versus Nondimensional Velocity	48

(Continued)

LIST OF ILLUSTRATIONS (Concluded)

Figure		Page
22.	Force Versus Nondimensional Velocity	49
23.	A Typical Cylinder Before Impact	59
24.	Shot Number 12 After Impact.	60
25.	Shot Number 11 After Impact.	61
26.	Shot Number 45 After Impact.	62
27.	A Close-up Illustration of a Failed Area on Shot Number 45.	63
28.	The Impact End of Shot Number 45	64
29.	The Air Gun.	65
30.	Motion Picture of an Impact.	66
31.	Motion Picture of an Impact.	67
32.	Motion Picture of an Impact.	68

SUMMARY

A dimensional analysis is performed for the case of a circular cylindrical shell impacting on a rigid target. It is found that for any given material, the velocity at which failure occurs is a function of the thickness to diameter and length to diameter ratios. Failure of a shell is defined as the appearance of a crack through which a light placed within the shell can be seen from the outside.

Experiments are performed to determine the form of the equation relating failure velocity and shell geometry. A new technique for the photogrid method of strain measurement is discussed. Other instrumentation used includes the Hopkinson pressure bar for measuring impact force and high speed photography for qualitative study of impact phenomena.

It is found that the empirical equation

$$V\sqrt{\frac{\rho}{\sigma_f}} = 0.6354\,\frac{Lt}{D^2} + 49.287\,\frac{t^2}{D^2} - 0.1095\,\frac{L}{D} - 12.970\,\frac{t}{D} + 1.297$$

fits the data with good accuracy in the region $2.7 \leq \frac{L}{D} \leq 10.7$, $0.045 \leq \frac{t}{D} \leq 0.126$, using AISI 4130 steel shells. Plots of strain versus non-dimensional length and of impact force versus non-dimensional impact velocity are presented. It is noticed in the force versus velocity curves that force increases directly with velocity up to a certain point, then drops sharply and stays at a relatively constant value. Values of force are seen to agree reasonably well with classical bar impact theory.

LIST OF SYMBOLS

Symbol	Definition
A	Cross sectional area
d	Distance
D	Shell diameter
E	Modulus of elasticity
E'	Plastic modulus
GF	Gage factor
L	Shell length, length
P	Average impact force
R_c	Value of the calibration resistor
R_g	Resistance of the gage
t	Shell thickness
T	Impact duration, time
V	Failure velocity
δ_c	Deflection of the voltage pulse caused by a dummy strain
δ_E	Deflection of the voltage pulse caused by impact
ϵ	Strain
ϵ_c	Calibration strain
ϵ_E	Strain caused by impact
γ	Poisson's ratio
ρ	Density
σ	Stress
σ_f	Ultimate stress of the material

CHAPTER I

INTRODUCTION

Purpose of the Research

Since the inception of the United States space program, it has become apparent that a compact and lightweight source of auxiliary power for rockets and spacecraft is required. This requirement is easily met by certain types of radioisotope power generators and nuclear reactors. However, the use of a nuclear power source in a space vehicle requires that the radioactive fuel be contained in a capsule which will maintain its integrity despite any conceivable type of accident during or before flight. In particular, it is necessary that no fuel be released at the surface of the earth during a high velocity impact.

The present state of knowledge in the fields of dynamic stability of shells, large deflection theory, and high strain rate properties of materials precludes the attack on this problem by exclusively theoretical means, and suggests that an experimental study be made.

One method of experimental analysis of the problem would be to perform a program of tests studying the effects of the following variables on the failure velocity of structures:

a. specimen geometry
b. material properties
c. angle of impact
d. target properties
e. filler material properties
f. temperature
g. scale factors

However, it is felt that such a program would require a prohibitive number of tests and time, and that the resulting empirical relationship would either be so complicated or so arbitrary as to be useless.

It is proposed here to take the opposite approach and to study the simplest case of any practical value: the axial impact of an empty cylindrical 4130 steel shell on a plane target. Open ends are chosen for ease of construction. It is hoped that this research will provide a foundation for further theoretical studies, and that it will provide a basis for the eventual complete solution of the problem.

It has been noted in the impact literature that there are in general very few methods for taking quantitative data in impact studies. A comprehensive description of the Georgia Tech Impact Laboratory, set up in 1964-1965, a discussion of experimental techniques and apparatus, and the development of some new techniques is included herein.

Definition of the Problem

The problem was to study some of the geometrical factors which affect the structural integrity of an open ended cylindrical shell under impact loading, using dimensional analysis in addition to experimental techniques. A computer was then used to correlate undetermined constants in the dimensional analysis with experimental results.

Failure of a fuel container was arbitrarily defined thus:

A container is said to have failed if: a) There are obvious holes in the walls, through which a light placed inside can be seen from the outside, or b) there are numerous large cracks at approximately the same location on both the inside and outside surfaces.

History and Literature Review

Although the consideration of impact effects on shell structures did not appear in the literature until the 1950's, the consideration of the impact problem as a branch of rigid body dynamics appears in most elementary textbooks on physics. The rigid body problem was first considered by Galileo, who confused the concepts of momentum and energy. The first satisfactory solutions were provided by Newton (1), who also introduced the concept of coefficient of restitution. After these elementary treatments, it became apparent that the problem of impact on a body of a real material was in essence unsolvable in terms of the existing knowledge, and that it was necessary to study certain idealizations. Saint-Venant (2), and Boussinesq (3) considered axial impacts on solid bars in the elastic range, and developed basic concepts and methods which would be used in later investigations. After this, important concepts in impact were developed in the literature on wave propagation and vibrations of elastic bodies, and elastic stability theory. Later, the development of shell theory by such well-known persons as Aron, Love, Timoshenko, Vlasov, and Gol'denveizer allowed the solution of some of these problems for shells of very simple geometry.

The mathematical treatment of plastic wave propagation in a non-strain rate sensitive material was first presented in the classic work by Von Karman and Duwez in 1942 (4, 5) and triggered a flurry of debate and mathematical and experimental research on the question of whether materials were strain rate sensitive, and if so in what manner (6, 7). It was generally conceded that most engineering metals are in some degree strain rate sensitive, although there has never been a satisfactory

mathematical correlation of all of the parameters. The work of Malvern (8), however, postulated a simple mathematical relation among stress, stress rate, strain, and strain rate in terms of two arbitrary constants, and thus set the stage for the treatment of impact problems in strain-rate sensitive materials.

An important early work on the effects of impact on cylindrical shells was completed by Hodge (9), who used a rib-stiffened rigid-plastic model with no strain rate dependence, and classical shell theory. He considered "medium" and "high" loads, and "short" and "long" shells. Although he did achieve solutions, his work did little to advance the knowledge of the actual problem.

Berkowitz (15), in 1962, considered axial impact on a semi-infinite elastic membrane shell, using integral transforms to obtain a solution. However, it was impossible to invert the transforms unless a "long time" solution was assumed. Spillers (16), however, did a much more satisfactory analysis, using the method of characteristics, with a shell theory of Hermann and Mirsky (11, 12, 13) which included the effects of transverse shear and rotary inertia. Elastic and viscoelastic models were considered and short time solutions were found with the aid of a digital computer.

It should be noted that none of the literature cited has purported to solve the problem of a thick, finite length cylindrical shell, taking strain-rate theory into account in some satisfactory manner.

CHAPTER II

DIMENSIONAL ANALYSIS

As has been seen, although great advances have been made in the fields of wave propagation, dynamic stability theory, and analysis of large plastic deformations, the state of the art has not advanced sufficiently to yield theoretical results for the impact velocity at which a cylinder will rupture. Thus two choices remain: (a) perform a dimensional analysis, and base the conclusions solely on experiments, or (b) compare the results of the experiments with some simpler theory. The first method will be chosen.

The theory of dimensional analysis has been discussed extensively by several authors (17, 18, 19). Basically, it involves deciding, on the basis of experiment or experience, what parameters are involved in the solution of a certain problem, and then using the principle of dimensional homogeneity to group the parameters into dimensionless π groups, the number of π groups being equal to the number of parameters needed to describe the phenomenon considered minus the number of independent fundamental units needed in specifying the units of the parameters. Thus if K kinds of units are needed to specify n quantities, the equation is of the form

$$f(\pi_1, \pi_2, \ldots, \pi_{n-k}) = 0$$

which can be symbolically solved for any π group, π_α, thus

$$\pi_\alpha = F(\pi_1, \pi_2, \ldots, \pi_{\alpha-1}, \pi_{\alpha+1}, \ldots, \pi_{n-K})$$

Therefore, on the basis of experimental evidence and with the use of dimensional analysis, it should be possible to "solve" a problem.

A major difficulty with this technique is the trouble experienced in deciding which parameters to choose as important in the solution of a problem. A decision can either be made arbitrarily, based solely on experience and intuition, or it can be based on a partial or complete mathematical analysis of the problem or some similar problem. In either case, if too few variables, or incorrect variables are chosen, an incomplete analysis will result; while if too many variables are chosen, the result will be unnecessarily complicated.

In this case it is postulated that the failure velocity of an open-ended cylindrical shell is a function of the geometrical properties of the shell usually considered in thin shell theory and the properties of the material used. It is, therefore, necessary to consider a system of variables thus:

Symbol	Dimensions	Quantity Denoted
D	L	Shell Diameter
t	L	Shell Thickness
L	L	Shell Length
V	LT^{-1}	Failure Velocity
E	FL^{-2}	Elastic Modulus of the Material
E'	FL^{-2}	Plastic Modulus of the Material
σ_f	FL^{-2}	Ultimate Stress of the Material

ρ	FT^2L^{-4}	Density of the Material
γ	1	Poisson's Ratio

It is immediately noted that three fundamental units: force, length, and time, are required to describe the nine parameters chosen as pertinent; thus, there will be 9-3=6 π groups required. It is necessary that these groups be independent in the mathematical sense, that is, no group should be derivable from any other group or groups by any combination of the processes of multiplication, division and exponentiation.

It is now possible to use the scheme devised by Buckingham (18) to determine the form of the dimensionless groups. The three quantities, D, V, and σ_f, containing all three types of units, are arbitrarily chosen as redundant varibles. Dimensionless groups are then found. Thus

$$\pi_1 = D^{\alpha_1} V^{\beta_1} \sigma_f^{\gamma_1} \gamma \tag{1}$$

$$\pi_2 = D^{\alpha_2} V^{\beta_2} \sigma_f^{\gamma_2} \rho \tag{2}$$

$$\pi_3 = D^{\alpha_3} V^{\beta_3} \sigma_f^{\gamma_3} L \tag{3}$$

$$\pi_4 = D^{\alpha_4} V^{\beta_4} \sigma_f^{\gamma_4} t \tag{4}$$

$$\pi_5 = D^{\alpha_5} V^{\beta_5} \sigma_f^{\gamma_5} E \tag{5}$$

$$\pi_6 = D^{\alpha_6} V^{\beta_6} \sigma_f^{\gamma_6} E' \tag{6}$$

Working with equation (3), dimensions are substituted.

$$1 = L^{\alpha_1}\left(\frac{L}{T}\right)^{\beta_1}\left(\frac{F}{L^2}\right)^{\gamma_1} L^1$$

Equating exponents of F, L and T,

$$F: \quad \gamma = 0$$

$$L: \quad \alpha = -1$$

$$T: \quad \beta = 0$$

Hence

$$\pi_3 = \frac{L}{D} \tag{7}$$

and in a similar manner, working with equations (2)-(6),

$$\pi_1 = \gamma \tag{8}$$

$$\pi_2 = \frac{\rho V^2}{\sigma_f} \tag{9}$$

$$\pi_4 = \frac{t}{D} \tag{10}$$

$$\pi_5 = \frac{E}{\sigma_f} \tag{11}$$

$$\pi_6 = \frac{E'}{\sigma_f} \tag{12}$$

Since it is proposed to test shells of one material only, π_1, π_5 and π_6

can be considered to be constants. Relations of the form

$$f(\pi_2, \pi_3, \pi_4) = 0$$

are sought, which can be solved for π_2, thus

$$\sqrt{\pi_2} = g(\pi_3, \pi_4) \tag{13}$$

so that the failure velocity equation will be of the form

$$V = \sqrt{\frac{\sigma_f}{\rho}} \; F\left(\frac{L}{D}, \frac{t}{D}\right)$$

CHAPTER III

INSTRUMENTATION AND EQUIPMENT

Standard techniques in experimental studies of impact phenomena in the past have included using a large air gun as an efficient source of high velocity motion, and a Hopkinson Pressure Bar as impact force measuring device.

These two pieces of equipment were much the same as those used by Ripperger (20) and Karnes (21) at the University of Texas. In addition, a carefully synchronized high speed motion picture camera, and a new adaptation of the photogrid technique for plastic strain measurements were used. Impact velocities were measured by means of two photoelectric cells and an electronic timer. A floor plan of the experimental setup is shown in Fig. 1.

Air Gun

The air gun was of the type described in (22). Since it is not our purpose here to discuss design and construction of air guns, only pertinent operating details will be examined. Reference should be made to Fig. 2 for the following discussion.

Compressed air was produced by the compressor and stored in tank A. The actual operation of the gun was divided into three stages: set, charge, and fire. Tank B was maintained at a constant pressure of 300 psi. Valve 3 was first opened, putting a pressure of P_s into chamber D, and pushing piston P into the full forward position. Valve 3 was then

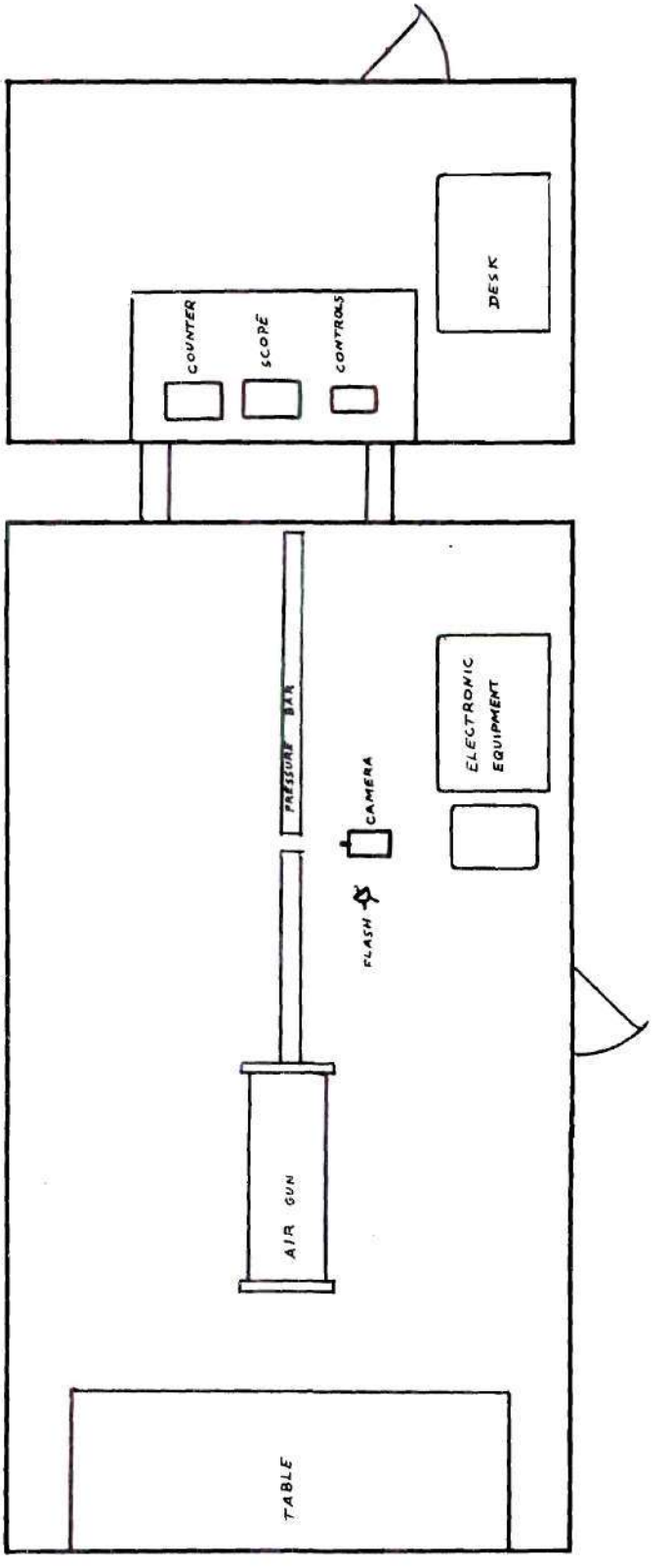

Figure 1. Floor Plan of the Impact Laboratory.

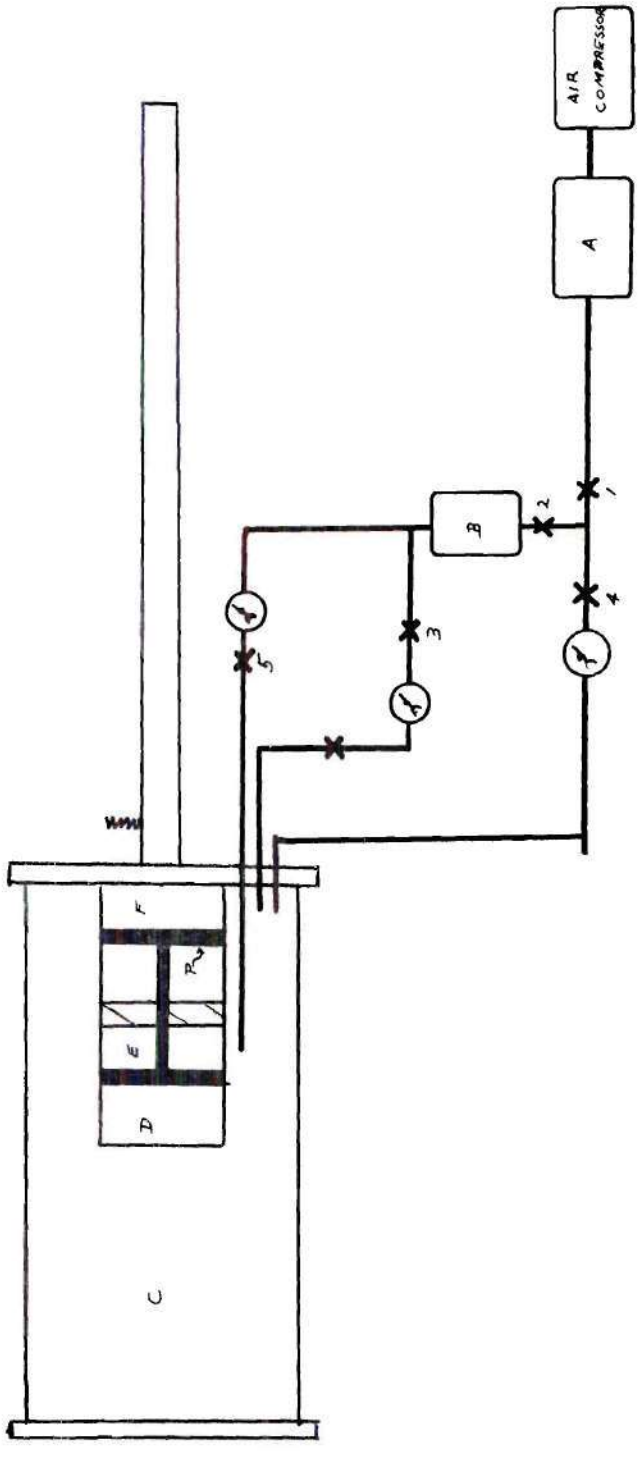

Figure 2. Operation of the Air Gun.

closed again. Air was then admitted into chamber C, by means of valve 4, producing a pressure P_c. Firing was accomplished by simultaneously actuating valves 5 and 6 electrically, thus filling chamber E and forcing piston P into the full back position. This caused a direct motion of air from chamber C through chamber F and into the barrel, where the projectile was held by the adjustable holding spring.

To get some idea as to the expected performance of this sytem, it was convenient to perform a dimensional analysis. The following were considered to be pertinent variables:

V_{el} - Final velocity of the projectile

V_c - Volume of chamber C

V_b - Volume of the barrel

M - Mass of the projectile

P_c - Initial pressure in chamber C

It was immediately apparent that there are 5-3=2, π groups. They were chosen arbitrarily as

$$\pi_1 = \frac{m\, V_{el}^2}{P_c\, V_c}$$

$$\pi_2 = \frac{V_c}{V_b}$$

Thus

$$\pi_1 = f(\pi_2)$$

or

$$V_{el}^2 = \frac{P_c V_c}{m} f\left(\frac{V_c}{V_b}\right)$$

However, since in this case V_c and V_b are constant, it was convenient to write

$$V_{el} = K_1\sqrt{\frac{P_c}{m}}$$

In order to add generality, another constant was added to form a general linear relationship between V_{el} and $\sqrt{\frac{P_c}{m}}$,

$$V_{el} = K_1\sqrt{\frac{P_c}{m}} + K_2 \tag{14}$$

An experimental investigation showed that equation (14) applies within very close limits for the range of pressures and masses usable in the system.

Only two other pertinent comments need be made about the operation of the air gun. The first is that the set pressure, P_s, needed to keep the gun from firing prematurely was found to be approximately

$$P_s \approx 0.4\, P_c$$

The other is that, due to the tendency of the gun to leak some air for high values of P_c, the compression in the adjustable holding spring had some effect on premature firing, also. No attempt was made to control this factor quantitatively.

Hopkinson Pressure Bar

The pressure bar technique was first used by B. Hopkinson (23) in 1913, and was revised and analyzed in great depth by R. M. Davies (24) in 1948. In the form Davies used it, the pressure bar was a long cylindrical rod. The specimen to be tested was impacted against one end, and the displacement of the other end was measured, using some suitable device. Then, elasticity theory was used to relate displacement of the measuring end to impact pressure and duration. The development of modern stress analysis equipment, notably the resistance strain gage and the cathode ray oscilloscope, have allowed further modernization of this equipment, thus providing greater precision and ease of use.

Physical Design of the Bar

The Pressure Bar, as used in these experiments, was a mandrel bar of Latrobe "Staminal" die steel, with an analysis of: carbon, 0.55 per cent; silicon, 1.00 per cent; manganese, 0.90 per cent; chromium, 0.40 per cent; nickel, 2.70 per cent; vanadium, 0.13 per cent; and molybdenum, 0.45 per cent. It was heat treated and quenched, thus providing a hardness of Rockwell 56-58 C. This allowed a great number of impacts under normally adverse conditions without damage, thus eliminating the need for a projectile end cap, as used by most investigators.

An experimental investigation by E. A. Ripperger (25) has indicated some of the criteria for design of pressure bars. He suggested that the diameter of the pressure bar should be the same as that of the impacting medium for maximum planeness of the stress wave front. Also to provide maximum response and minimum distortion, the bar should be no more than 1 inch in diameter. However, practical considerations demanded

that the bar used be somewhat greater in diameter than the specimens. For this reason a bar with diameter of 1.00 inch and a length of 10.0 feet was chosen.

The bar was encased in a thick-walled steel cylinder to provide sufficient mass to prevent excessive motion after impact, was supported by screws at several points, and the whole assembly was suspended from the ceiling by wires.

Strain Gage Apparatus

The magnitude of the stress pulse in the bar was measured by means of two electric resistance strain gages, mounted diametrically opposite each other, and connected so as to eliminate the effects of bending. Alternate gage locations were provided at 6, 12, and 18 inches from the impact end, but each location yielded essentially the same strain pulse. The gages were connected to a B.L.H. 10 channel switching and balancing unit, and excited by a 12 volt DC power supply.

The high speed phenomenon observed, however, did not allow strain read-out on the usual meter type instrument. Instead, it was necessary to use a Hewlett-Packard type 140A oscilloscope with a 1400A differential input amplifier. The oscilloscope trace was recorded on a Polaroid camera.

Proper oscilloscope triggering presented a major problem. The final solution involved using a third photocell setup, placed in front of the impact end of the pressure bar, and connected to the external trigger circuit of the oscilloscope.

Calibration was achieved by the method normally used in strain gage systems, that is, a set of precision resistors of known value were

arranged so they could be switched in and out of the system as "dummy" strains, in parallel with the strain gages.

Calculation of Impact Force

Impact force was calculated directly from the photograph of the oscilloscope trace using a one-dimensional strain theory and the definition of gage factor.

The gage factor is defined as

$$GF = \frac{\Delta R_G}{R_G \epsilon_c} \tag{15}$$

This factor is assumed to be constant and is furnished by the manufacturer with each package of gages. Although it is based on static measurements, several investigators, notably Nisbet, Brennan, and Tapley (26) have shown that in the frequency range below 20,000 cycles per second, the dynamic and static gage factors differ by less than five per cent.

Since connecting two gages to eliminate bending stress doubles the sensitivity of the system to tension and compression

$$\epsilon_E = \frac{\epsilon_c}{\delta_c} \cdot \frac{\delta_E}{2} \tag{16}$$

The normal stress-strain relation in one dimension is

$$\sigma = E_c \, \epsilon_E \tag{17}$$

By the definition of average stress,

$$\sigma = \frac{P}{A} \tag{18}$$

Solving (17) and (18) for P, the impact force is

$$P = E_c A\epsilon_E \tag{19}$$

Thus equation (15) can be used along with the known value of the calibration resistor to calculate ϵ_E, reading δ_c and δ_E from the oscilloscope and finally using equation (19) to calculate the impact force.

It is illustrative to perform a sample calculation using the data from shot number 37. The data was taken in the following manner: First, GF = 2.05 and R_G = 120.0 ohms were read from the strain gage package. Then, a calibration resistor of R_C = 1691.75 ohms was placed in the circuit, and with an oscilloscope sensitivity of 0.2 volts per centimeter, δ_c = 0.14 was read from the oscilloscope face. The oscilloscope settings were then changed to sensitivity 2 millivolts per centimeter, sweep time 0.2 milliseconds per centimeter. The specimen was impacted, and δ_E = 1 centimeter and impact time interval = 0.4 centimeter were read from the oscilloscope picture, Fig. 3. The pressure bar E_c = 30,000,000 pounds per square inch, and A = $\pi/4$ square inches.

There is now sufficient information to start the calculations. First use the formulas for the resistance of two resistors in parallel to obtain ΔR_G

$$\Delta R_G = R_G - \frac{R_G R_c}{R_G + R_c} \tag{20}$$

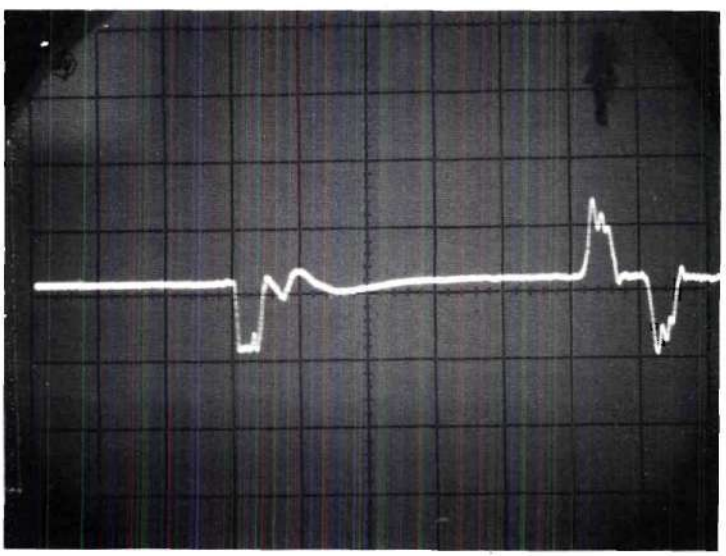

Figure 3. Strain Gage Oscilloscope Trace for Shot 37.

$$\Delta R_G = -7.948 \text{ ohms} \qquad (21)$$

The minus sign will be dropped for convenience. Substituting into equation (15) and solving for ϵ_c

$$\epsilon_c = \frac{7.948}{(120.0)(2.05)} = 0.00323089 \text{ inch/inch}$$

It is now possible to substitute into equation (26), making sure to convert δ_c and δ_E into the same units

$$\epsilon_E = 0.00323089 \left(\frac{1}{2}\right) \left(\frac{1 \text{ cm}}{10^3 \text{ cm}} \frac{2 \text{ volts}}{}\right) \left(\frac{\text{cm}}{0.14 \text{ cm } 0.2 \text{ volts}}\right)$$

$$\epsilon_E = 0.00015389 \text{ inch/inch}$$

Thus equation (19) yields

$$P = (30{,}000{,}000) \left(\frac{3.14}{4}\right) (0.000115389)$$

again replacing the minus sign

$$P = -2718.78 \text{ pounds}$$

The impact duration is

$$T = (0.4 \text{ cm})(0.2 \text{ millisecond/cm})$$

$$T = 0.08 \text{ millisecond}$$

It should be noted that equation (20) is sensitive to small errors in

R_g and that for the result to have any physical meaning, the computation must be carried out to a great number of significant places. Also, the value of R_c must be measured very carefully, and the effect of lead wire resistance must be added to it.

Photogrid Process

One of the simplest and most obvious methods of determining finite plastic strains on a large body is known as the grid process. It consists of simply affixing some sort of coordinate system to the body to be studied, applying the required loads to cause plastic deformation, then measuring the changes in the coordinate system by the use of some suitable instrument. However, the process has never been widely used because of the difficulty of applying a suitably accurate and indestructible grid to the actual body. The methods of applying grids used in the past include

Hand Scratching or Machine Scribing

These techniques, although presenting good accuracy, are difficult to perform, and since they require trained personnel and precision machinery, are quite expensive, especially if it is necessary to test a large number of models. In addition, scribed or scratched lines, since they may cause artificially high stress concentrations could affect the failure characteristics of the specimens.

Ink Drawing

This method is usually used in conjunction with rubber specimens, and can be considered to be a technique of model testing. It is not applicable to metal prototypes. A nicely worked out example of this type

of test may be found in (27).

Rubber Threads

This method has only been applied to soft porous materials. It is time-consuming and inaccurate, and is in general inapplicable to metal prototypes.

Photogrid Process

The ease of applying accurate photographic grids to a large number of prototypes, and their usual thinness and toughness, immediately marks the photogrid process as an obvious modification of the grid method of stress analysis. Its disadvantages in the past have been the toxic solutions required, the high pressure atomizing gun needed for correct application, and the difficulty of applying grids on curved surfaces.

History

The development of effective methods of application of photogrids did not begin until the science of photography was sufficiently advanced. The first two major papers on the subject are (28) and (29). In the 1940's a wealth of literature appeared, mostly concerned with the application of the technique to the analysis of deep drawing strains. Most of the early investigators used a formula which had the following composition:

Water	28 parts
Photoengraver's glue	4 parts
Ammonium Bichromate	1 part
Strong Ammonia Water	$\frac{1}{4}$ part

A later and more sophisticated process incorporated its own dye and eliminated the albumin-based viscid fluid called photoengraver's glue.

Its formula was:

Distilled Water	660 grams
Polyvinyl Alcohol	70 grams
Potassium Chromate	3.5 grams
Nigrosine Dye	30 grams
Duponol (L144 WD) Plasticizer	3 grams

This, too, had disadvantages. The formulas as given yielded a solution that was too viscous to spray on, too slow-drying to paint on, and even more slow-drying when mixed with water. It was insoluable in the common hydrocarbon solvents and was polymerized by alcohols, aldehydes, and ketones, with the exception of formaldehyde, which was considered undesirable for spraying.

McLaren (30) used a variation of the Kodak Transfax process; however, his work was apparently ignored because, much later, even expert workers in the field, such as Miller (31), were using photoengraving processes.

The resistance type strain gage was invented in the late 1930's, and by the end of World War II, the interest in this new method of strain measurement became so great that the photogrid process was largely ignored. In recent years, however, research in such fields as large plastic strains and dynamic buckling, in which the strain gage is virtually unusable, has become important. The photogrid process is well suited for use in these fields and is again coming into favor.

The Ortho-Resist Process

Probably the best method of application of photogrids is a process called Kodak Ortho Resist, which was developed by the Eastman Kodak

Company for use in photoetching and photomilling processes. It is inexpensive, safe, easy to use, readily available, and allows application of grids which are greatly superior to those applied by other methods. Until now, however, no mention of its use could be found in the experimental stress analysis literature. For this reason, the application of this technique to stress analysis will be discussed in considerable detail.

Choice and Preparation of the Negative. The choice of a grid pattern depends on the symmetry characteristics of the body to be studied. Thus, a bar or beam might require a rectangular coordinate grid, while a circular plate, on the other hand, is better suited to a polar coordinate system. The great versatility of the process would even allow different types of coordinates on different parts of the prototype.

Coordinate systems are most easily prepared by one of two processes. A very accurate grid is obtained by making a very large ink drawing, then reducing it photographically. This method has the added advantage of allowing very thin coordinate lines to be reproduced. The other method of preparing grids of high accuracy, although with thicker coordinate lines, is simple 1:1 reproduction of a standard type of graph paper. The coordinate system is photographed with a standard large-size reproduction camera, using a high contrast fine grain film. The negative thus produced is used directly in application of the grid.

Surface Preparation. In general, the procedure recommended by Kodak is unnecessary in stress analysis applications. Instead, a simple three-step procedure is quite sufficient.

The surface is first degreased by any available convenient process. Kerosene or some commercial degreaser is quite satisfactory as is methyl ethyl ketone or acetone. The surface is rubbed with a clean cloth and the solvent until it feels clean to the touch. In many cases, the degreasing step is not necessary at all.

The surface is then cleaned of any protective coating by rubbing with clean sandpaper or steel wool. This also removes outer oxide layers and adsorbed air. It is desirable to have a relatively smooth surface in order to obtain high image resolution, however, the resist emulsion will not adhere well to a very smooth surface without some modification. The exact type of surface finish required for a particular application is best determined by a trial and error process.

Finally, all surface grit is removed and oxidation is prevented by storing the prototype in a solvent until shortly before coating with the resist. For this purpose a clean, volatile solvent such as methyl ethyl ketone or alcohol is preferred.

Applying the Resist. The desirable properties of a resist coating for photogrid application are thinness and evenness. This gives best sensitivity characteristics and highest resolution. The sensitized solution should consist of: Kodak Ortho Resist, 1 part; and Kodak Photo Resist Thinner, 2 parts. This is mixed thoroughly and applied to the cleaned surface by wiping on with clean cotton balls, being careful not to touch any already coated surface with your fingers. The surface should then dry twenty to thirty minutes before exposure.

Although it is possible to perform the whole process under dim tungsten lamps, probably the best lighting source to use is commercial

red bulbs. The resist emulsion is almost completely insensitive to red light, and 100 watts of red illumination can be used for over an hour without harmful effect.

Safety in this case is a small matter. However, since volatile materials are used, it is wise to use a small industrial gas mask during the coating process. In a well ventilated darkroom, even this precaution is unnecessary.

Applying the Grid. Most of the experimenters in the past, (30), (31) have secured the grid negative to the specimen by means of a vacuum frame, making the exposure with electric arc lamps. However, the use of a plane frame is not applicable in the case of cylindrical shells. Since the only requirement is intimate contact between the negative and the specimen, it was found that a careful job with cellophane tape was quite acceptable. The grid negative is applied with its emulsion side in contact with the resist surface. Exposure is made with a standard photoflash bulb, thus eliminating the inconvenience of using an arc lamp. Some trial and error is involved in finding the correct amount of light to apply to the surface.

Development and Dying. Development and dying are carried out as recommended by Kodak: two to three minutes in Kodak Ortho Resist Developer, a running water rinse, then one minute in Kodak Photo Resist Dye. Ten minutes of drying at room temperature is sufficient to ensure a permanent image.

Image Measurement. It is imperative that, after the grid is applied and before straining, the grid be measured as a reference. Line thickness and grid uniformity must be taken into account. Measurements

are also made after straining. Strains are then calculated by the standard strain gage rosette formulas.

In this particular application, the grids were of sufficient uniformity that initial measurements were unnecessary. Measurements were made with a Bausch and Lomb shop microscope, with divisions readable to 0.001 inch.

High Speed Motion Pictures

Although the equipment necessary to record sufficiently the whole impact event was not readily available, it was possible to reconstruct the occurences in the phenomenon with the aid of a number of motion picture sequences. A Wollensak Fastax WF5 motion picture camera was used. This provided a framing rate of 6000 frames per second, while retaining the advantage of large frame size, thus, providing maximum information storage capacity. Effective shutter speed at this rate, as given in the Wollensak literature, was 1/18,000 second. Assuming the projectile was traveling 360 feet per second, it can be seen that during one frame, it would move a distance of

$$d = (360)(1/18,000)$$

$$d = 1/50 \text{ ft.}$$

or about $\frac{1}{4}$ inch. This was judged to be too much blur to produce useful quantitative information.

The solution to this problem was to use a model 501 Stroboflash supplied by Edgerton, Germeschausen, and Grier, Inc., with flash synchronized to camera framing by means of a magnetic pickup. This provided an

exposure time of 1.2 microseconds, which would yield a subject movement of

$$d = (360)(1.2/1,000,000) = 0.000432 \text{ ft.}$$

or about 0.005 inch.

Synchronization of the impact, the flash, and the camera was achieved with the aid of a Wollensak WF301A "Goose" control unit. The camera was started considerably (about 0.8 second) before the impact. The event sequence, controlled by the pushing of one button and occurring in a darkened room, was:

1. Close firing button
2. Supply camera with 280 volts
3. Open solenoid valves on the gun by 120 volt pulse, thus firing the projectile.
4. Start flash
5. Impact occurs
6. Turn off all equipment

The films thus exposed were developed to negatives and examined on a standard microfilm reader.

CHAPTER IV

RESULTS

Based on the failure criterion, the equation for the velocity at which failure occurs, fitted by the method of least squares, is

$$\sqrt{\pi_2} = 0.6354\ \pi_3\ \pi_4 + 49.287\ \pi_4^2 - 0.1095\ \pi_3 - 12.970\ \pi_4 + 1.297 \tag{22}$$

with the dimensionless quantities

$$\pi_2 = \frac{\rho V^2}{\sigma_f}$$

$$\pi_3 = \frac{L}{D}$$

$$\pi_4 = \frac{t}{D}$$

This curve was fitted using the program described in Burroughs Corporation Technical Bulletin number 168, "Nonlinear Least Squares Curve Fitting Using Algol on the Burroughs 220 Computer." The results (print out) given by this program are reproduced in Table 1.

In order to give a physical meaning to equation (22), Table 2 gives the predicted failure velocities for the nine sizes of cylinders tested, while Fig. 4 presents Table 3 in graphical form.

Some typical plots of axial plastic strain against nondimensional

length along the bar are shown in Figs. 5-19.

Graphs of impact force versus nondimensional impact velocity are given in Figs. 20-22. Rebound velocity was judged to be negligible on the basis of the high speed motion pictures.

There are clearly an insufficient number of points to plot accurate curves, especially in the low velocity range where no testing was done However, the curves are probably of the configuration shown.

A complete summary of the experimental results is given in Table 3. This table was computed with the aid of the equations given in Chapter III.

Tables 4 and 5 are transcriptions of typical data sheets.

Figures 23-28 illustrate typical post-impact configurations. Figure 29 illustrates the air gun and part of the experimental facility. Some typical impact motion pictures are shown in Figs. 30-31.

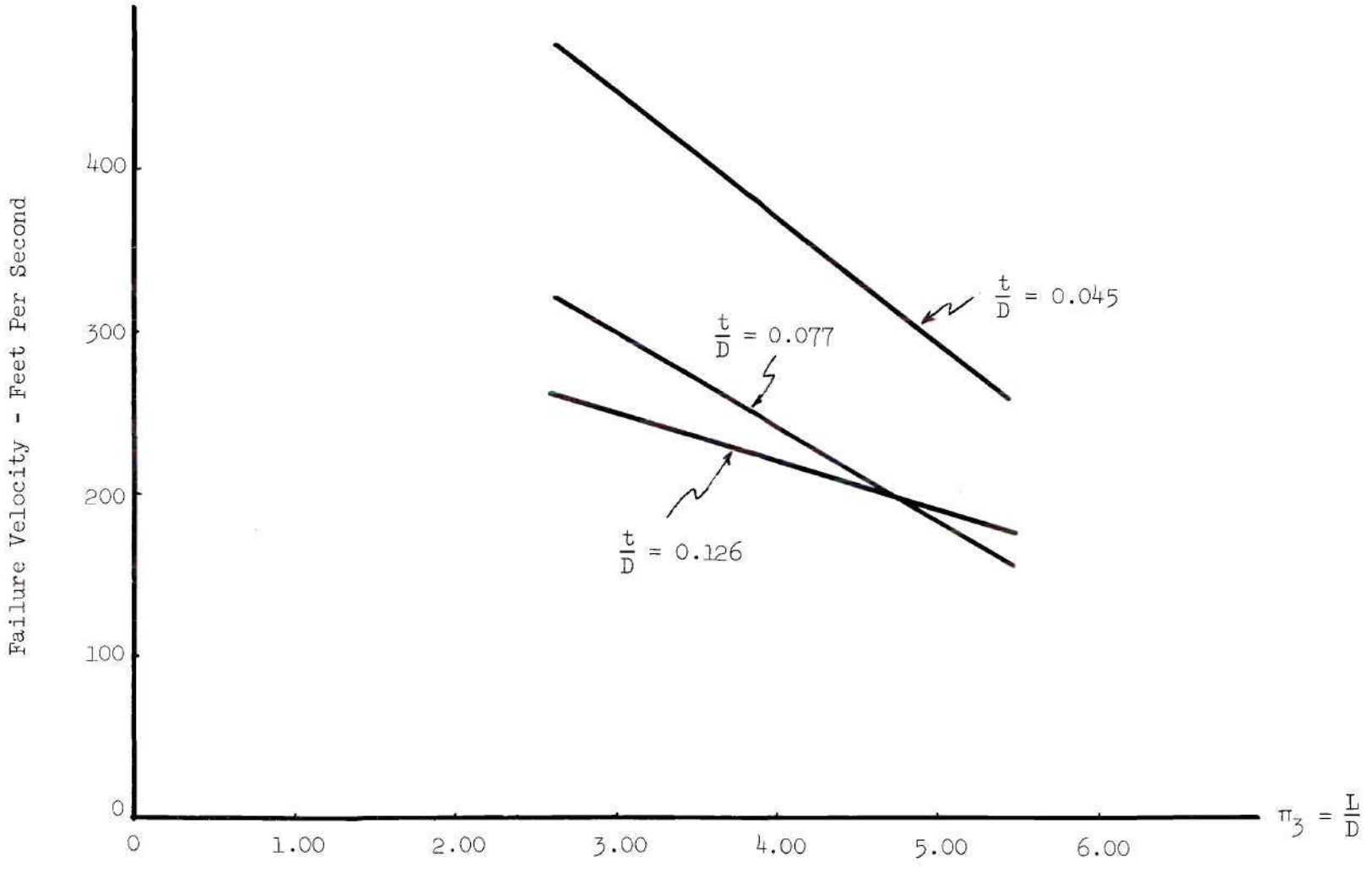

Figure 4. Failure Velocity as a Function of $\frac{t}{D}$ and $\frac{L}{D}$.

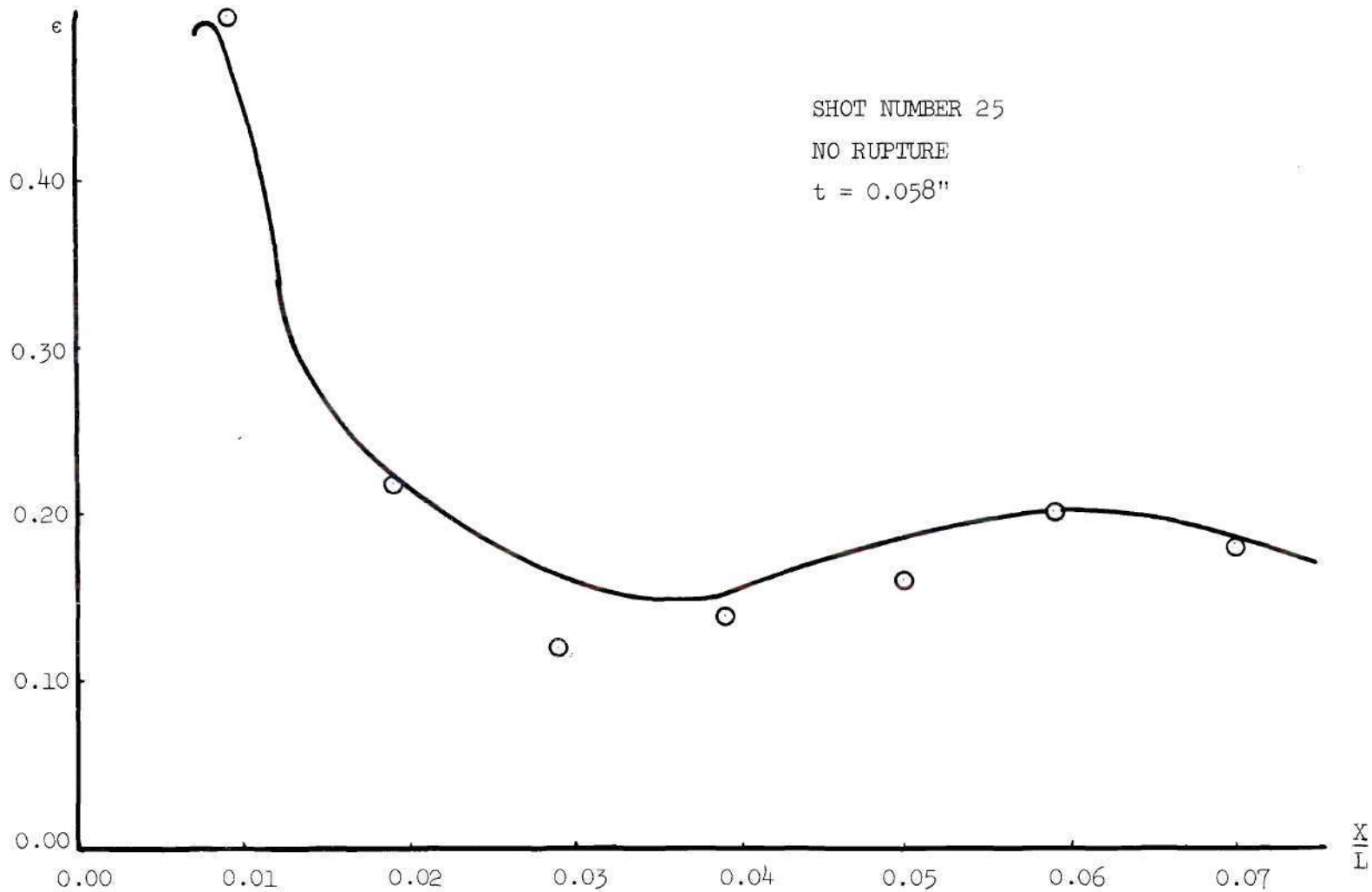

Figure 5. Strain Versus Nondimensional Length.

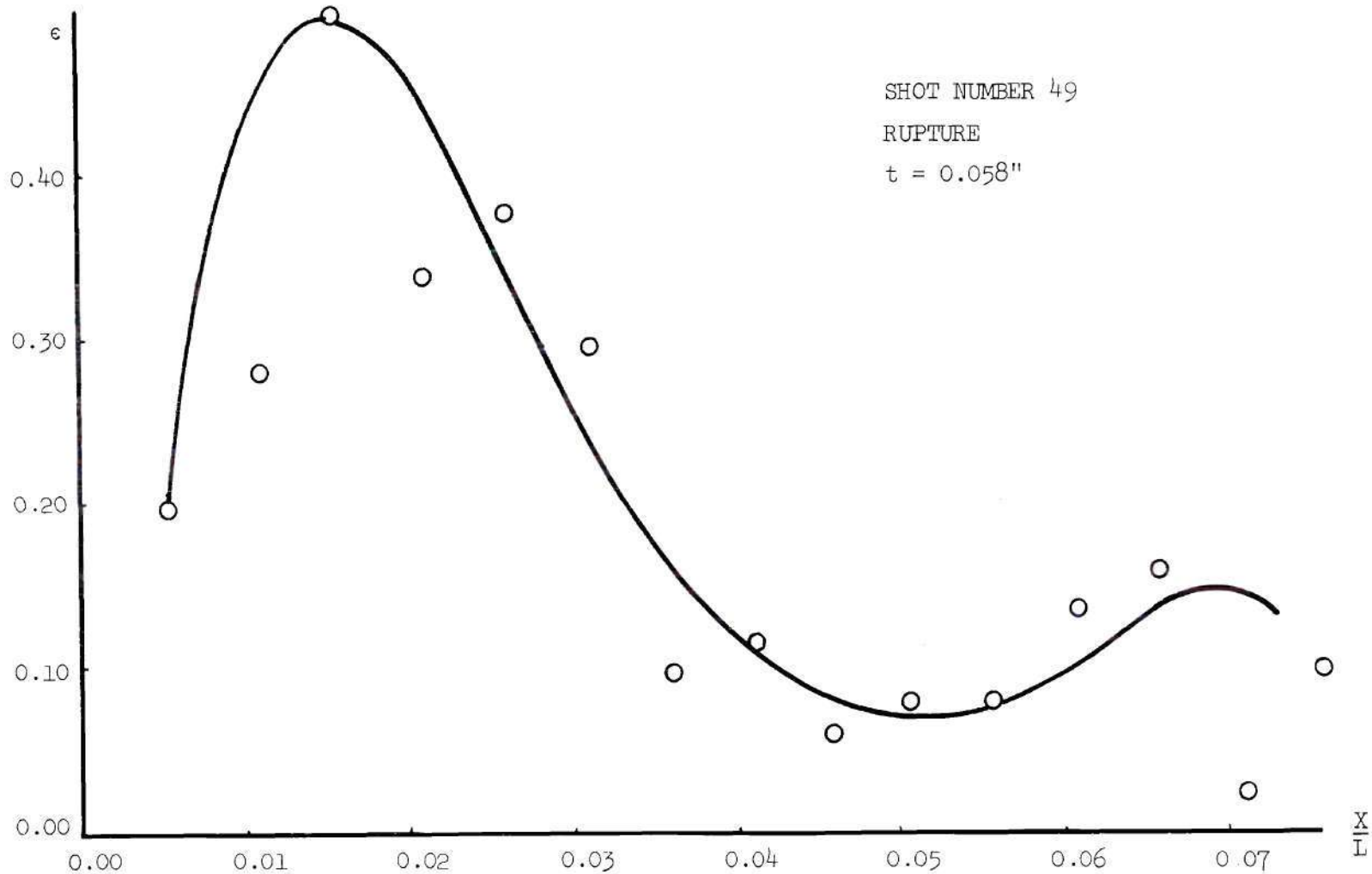

Figure 6. Strain Versus Nondimensional Length.

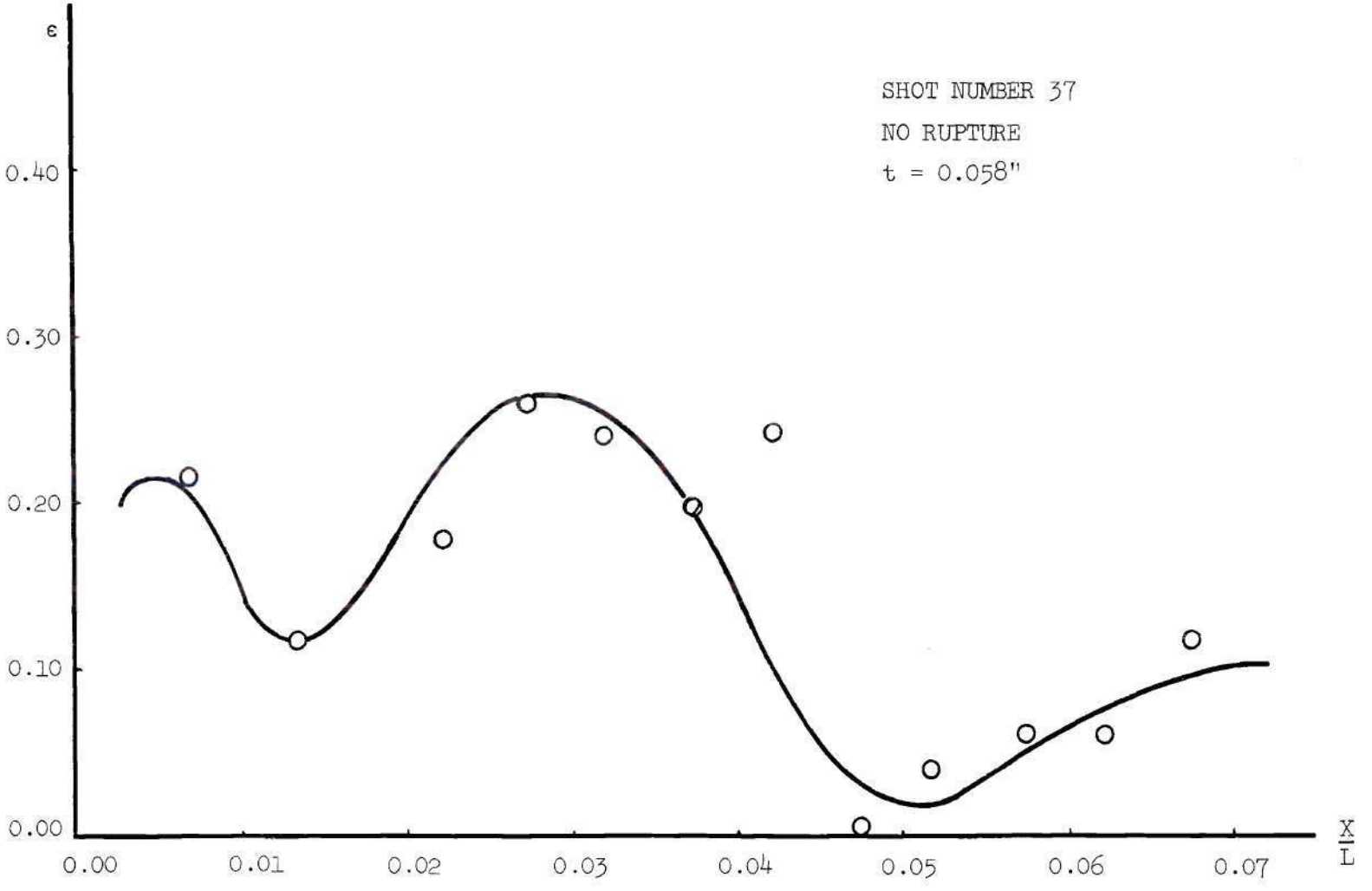

Figure 7. Strain Versus Nondimensional Length.

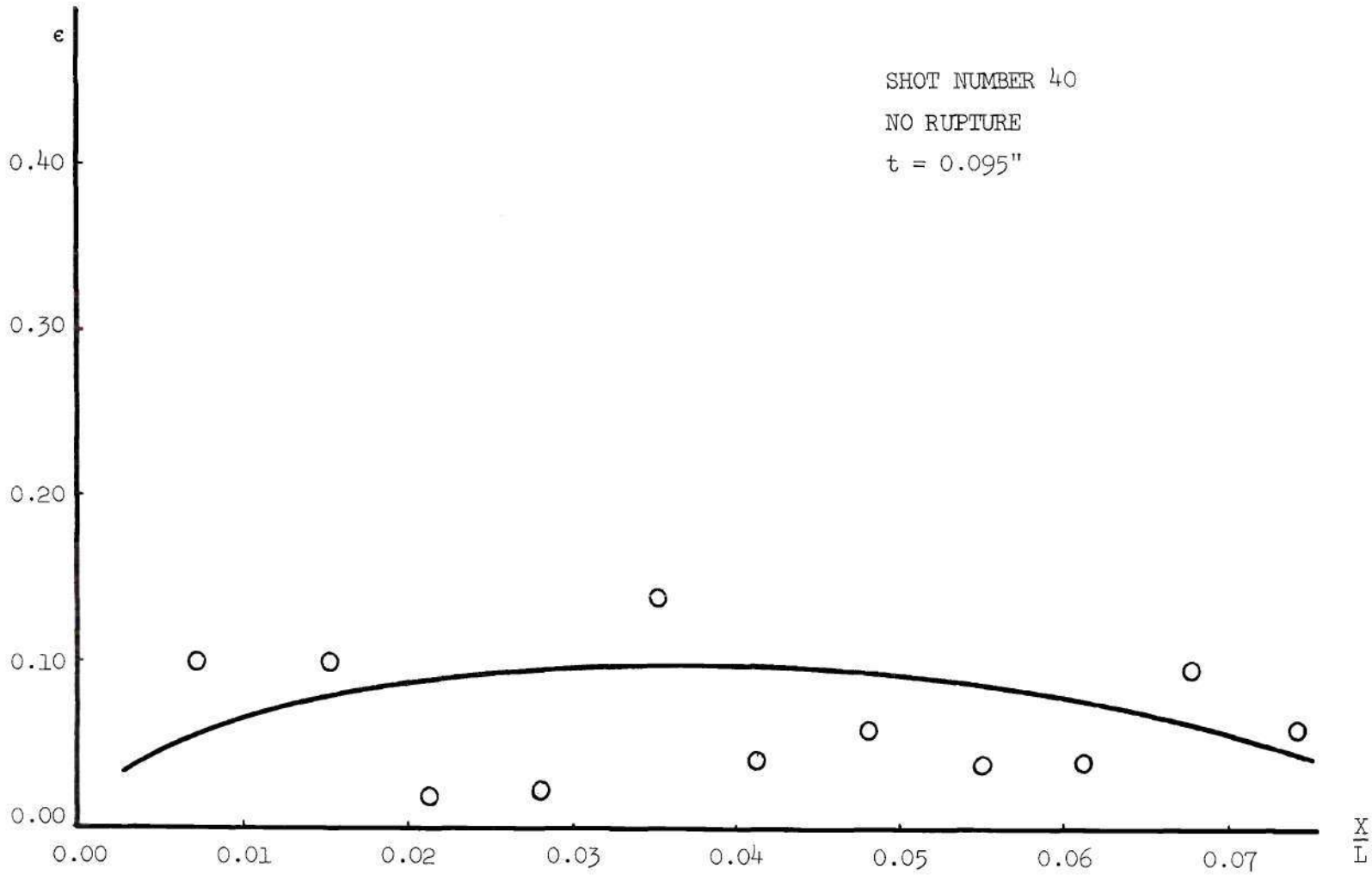

Figure 8. Strain Versus Nondimensional Length.

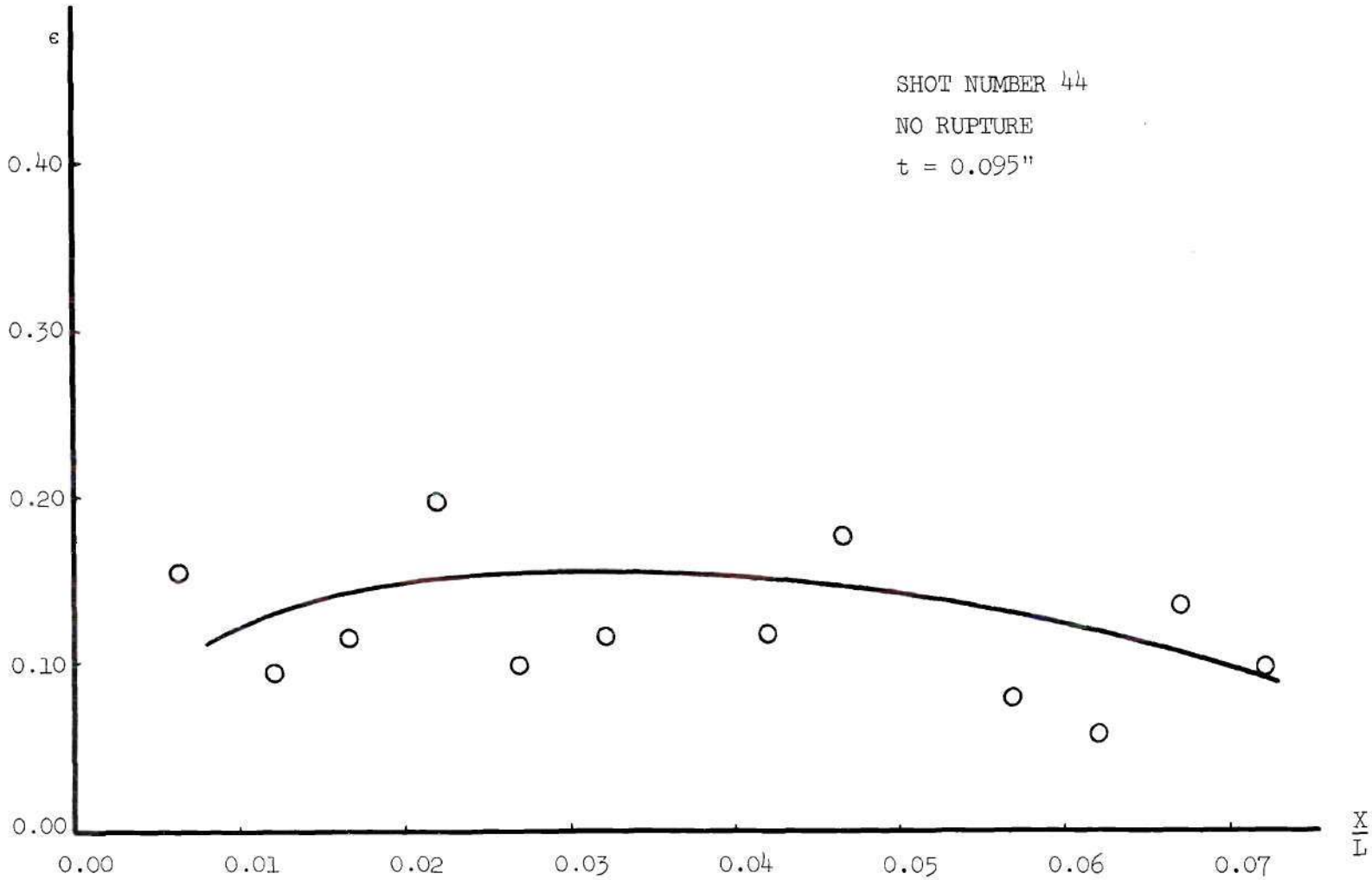

Figure 9. Strain Versus Nondimensional Length.

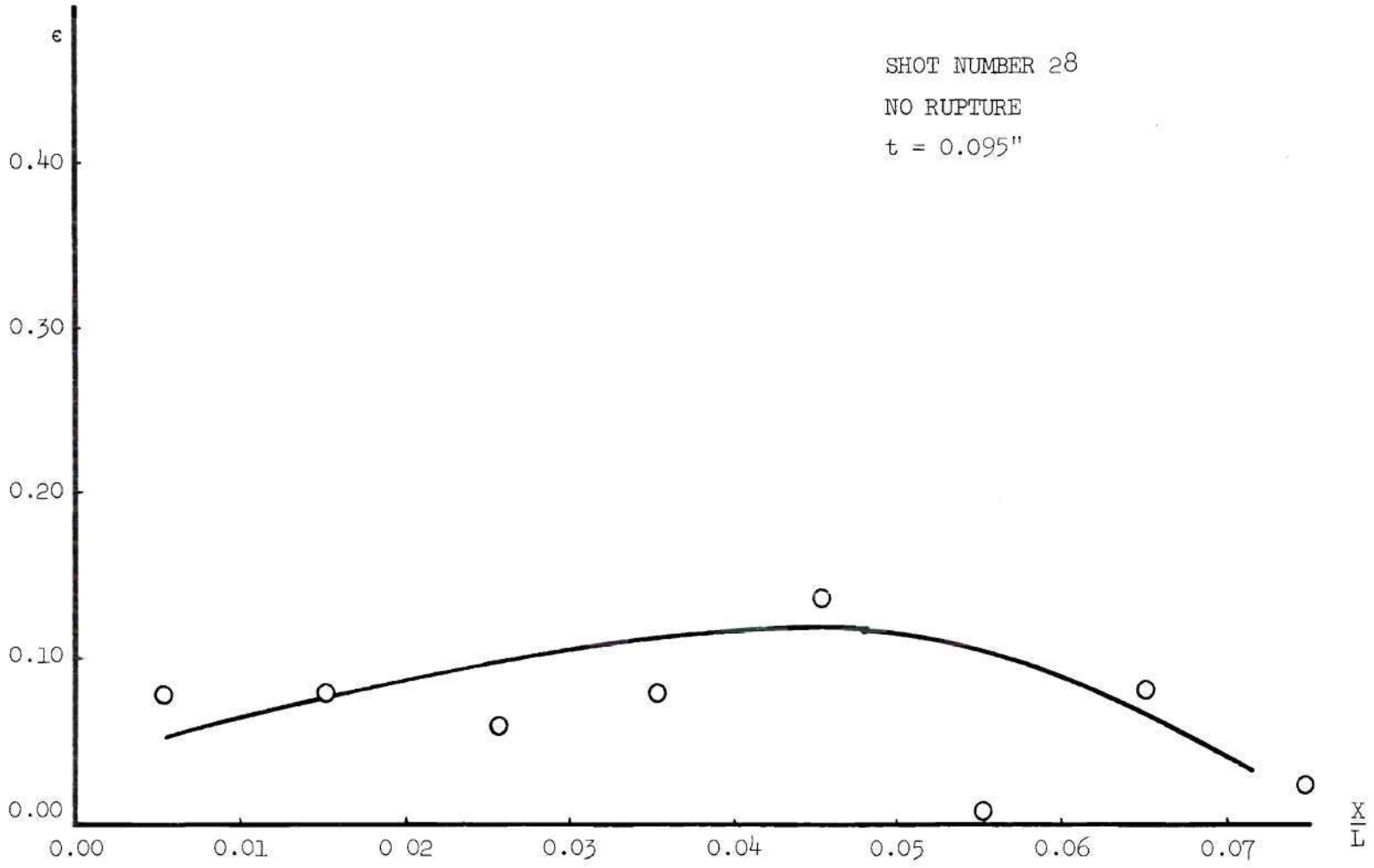

Figure 10. Strain Versus Nondimensional Length.

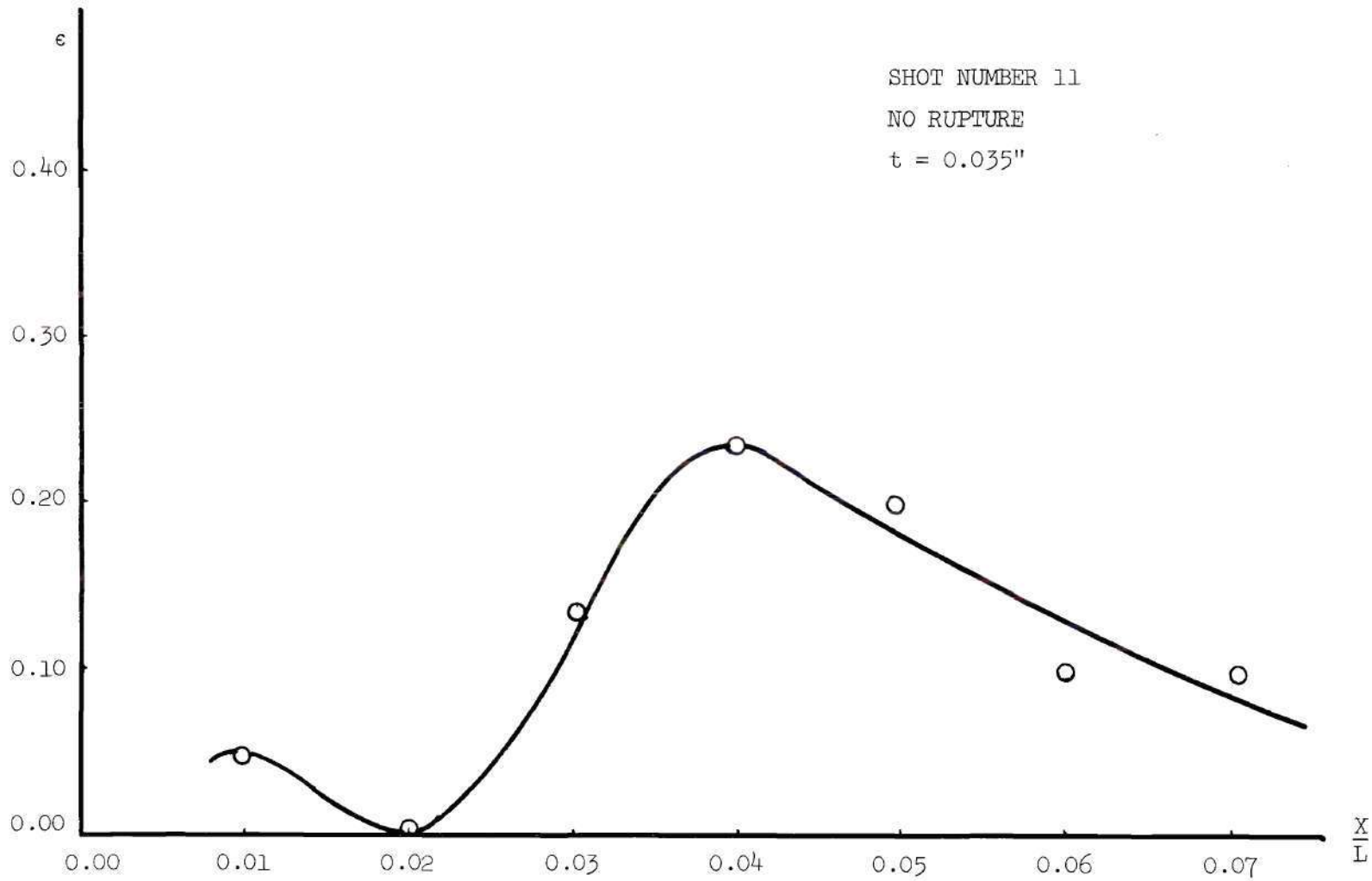

Figure 11. Strain Versus Nondimensional Length.

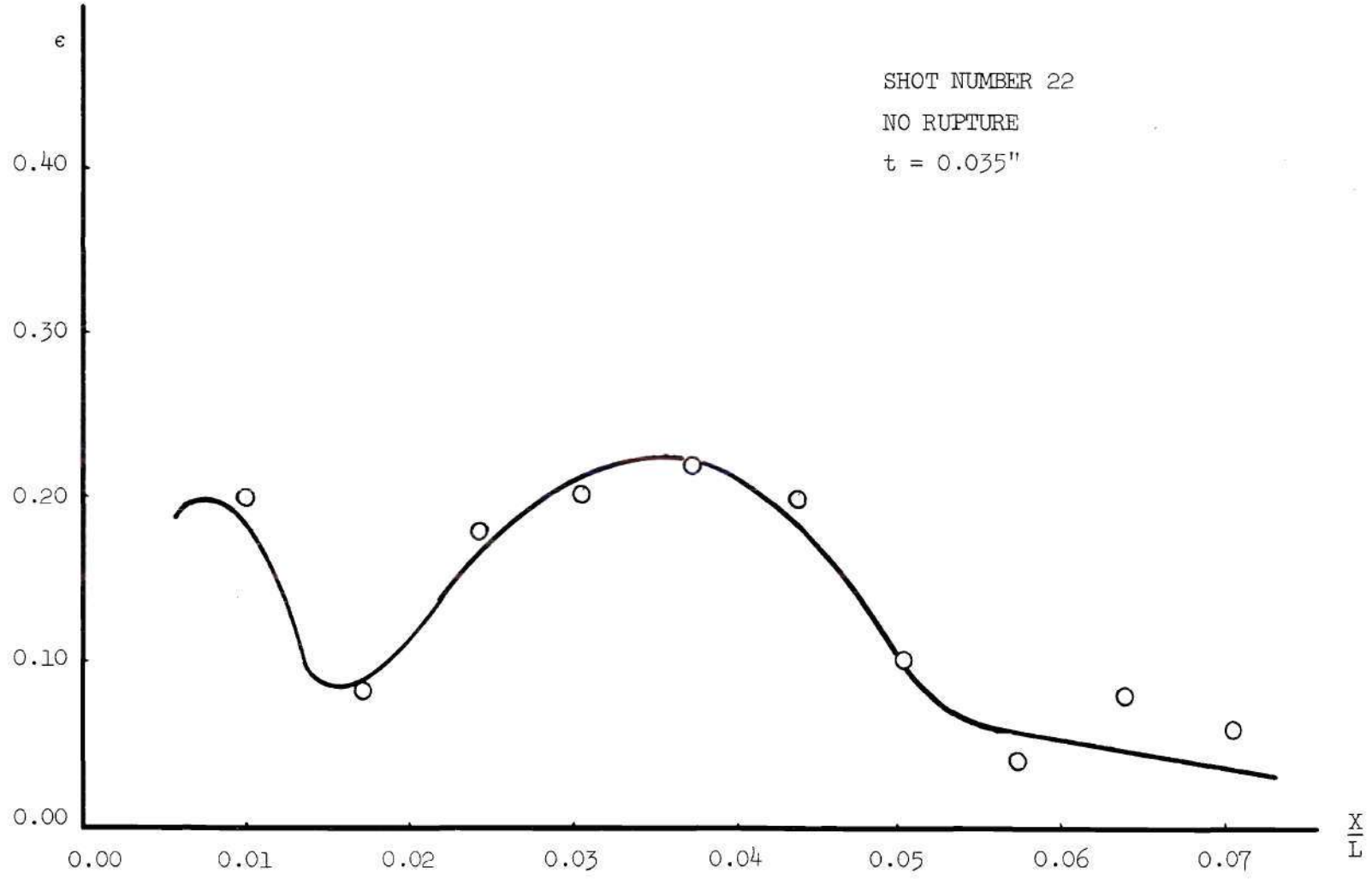

Figure 12. Strain Versus Nondimensional Length.

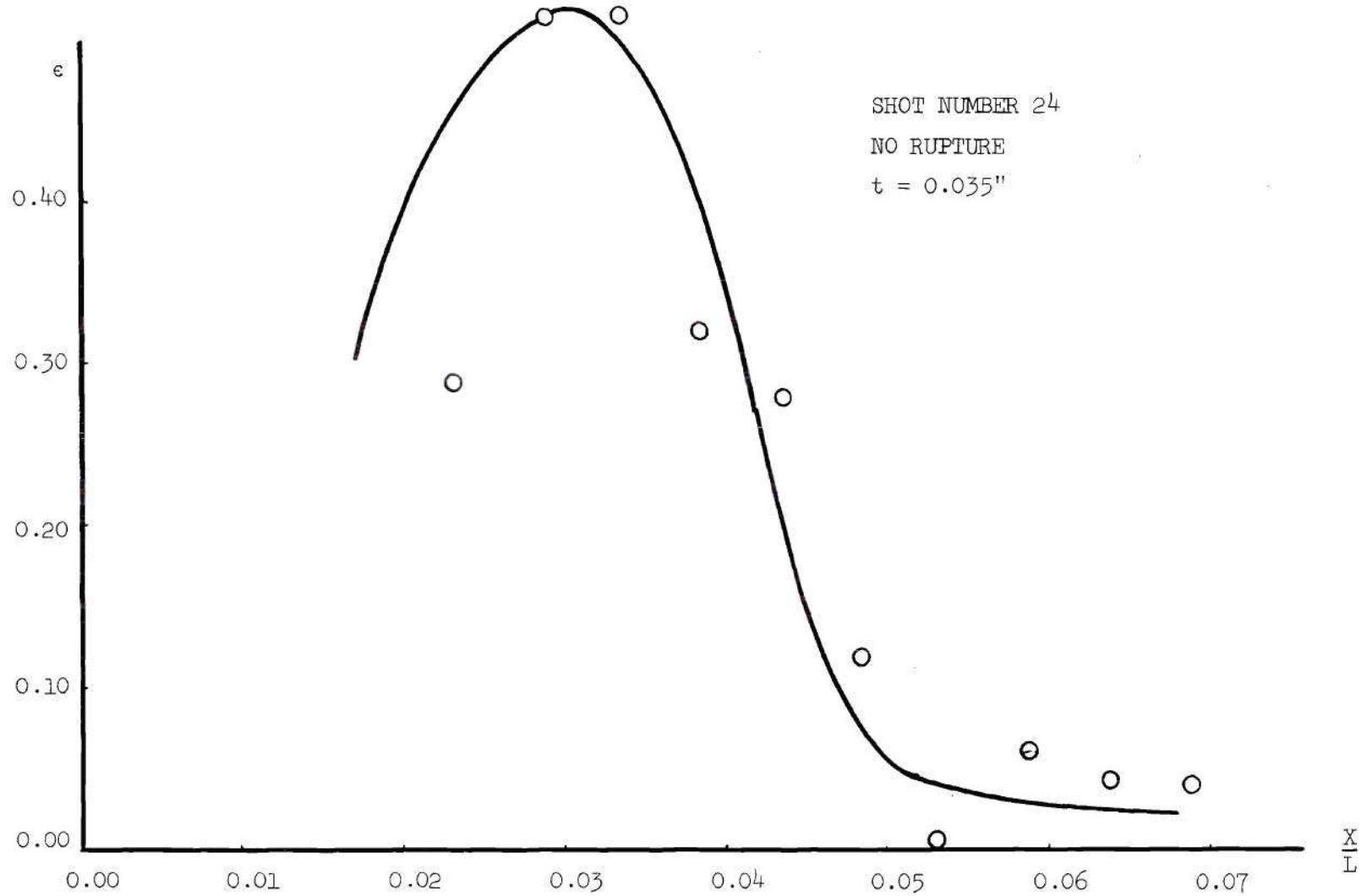

Figure 13. Strain Versus Nondimensional Length.

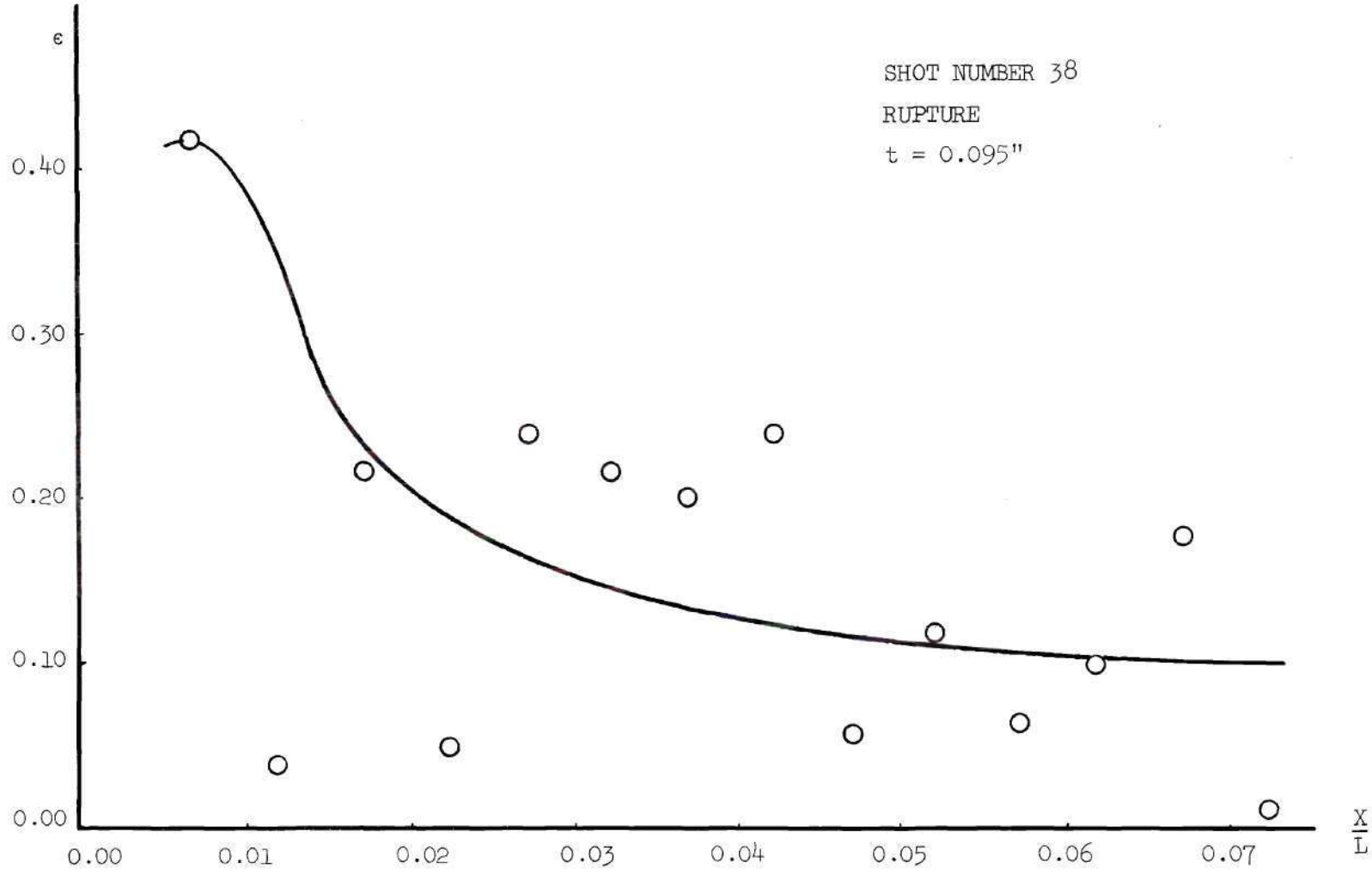

Figure 14. Strain Versus Nondimensional Length.

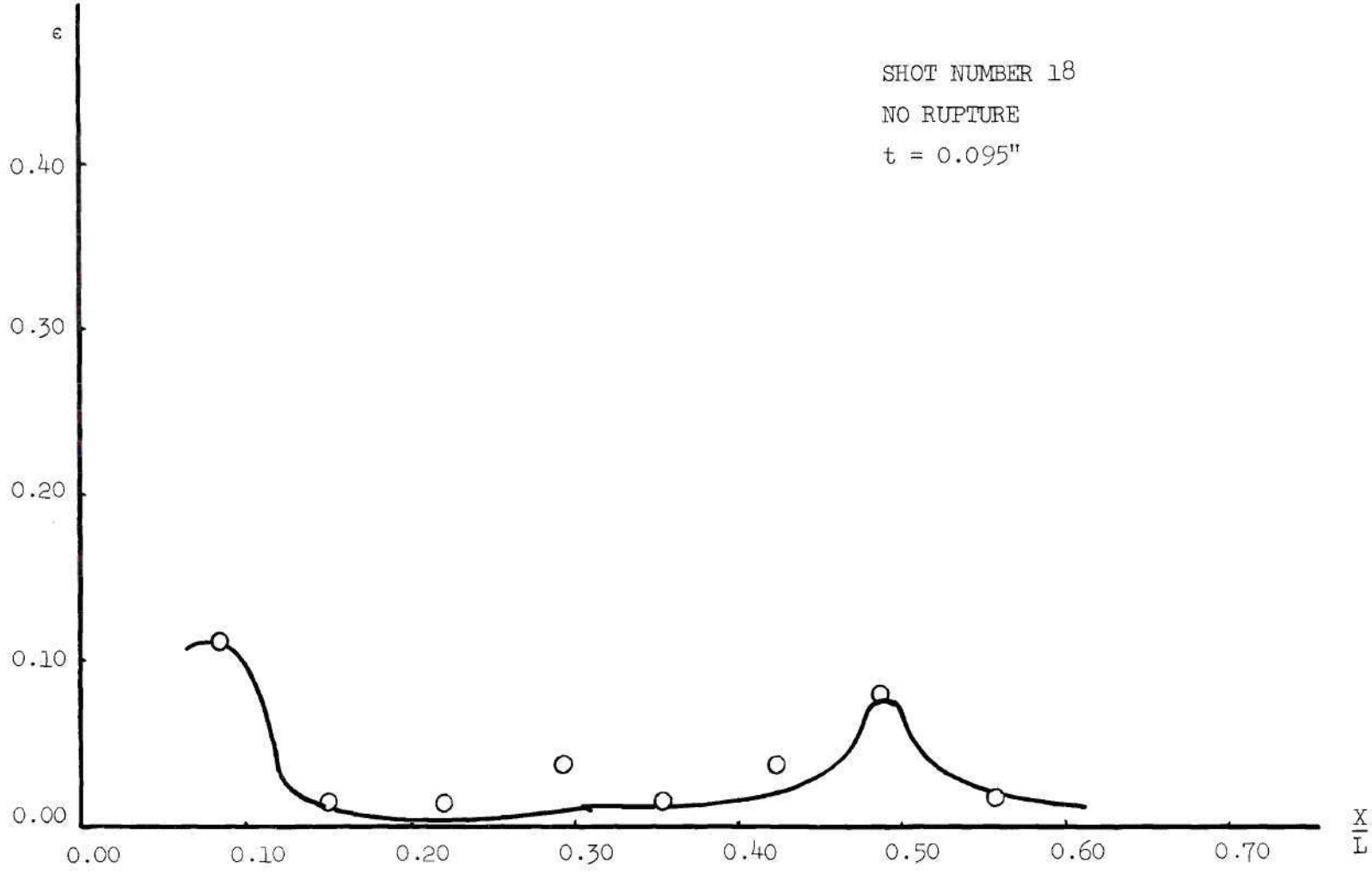

Figure 15. Strain Versus Nondimensional Length.

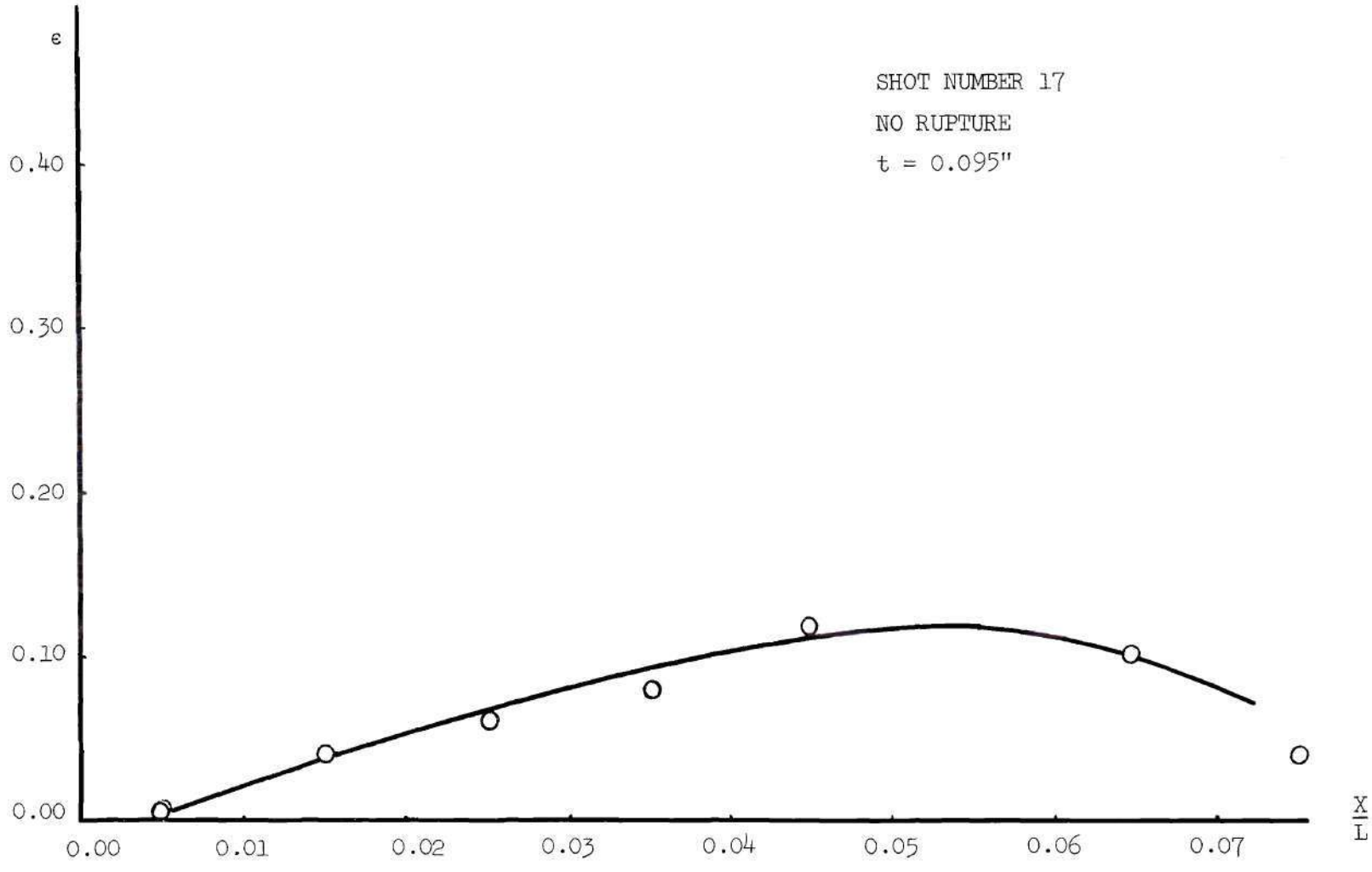

Figure 16. Strain Versus Nondimensional Length.

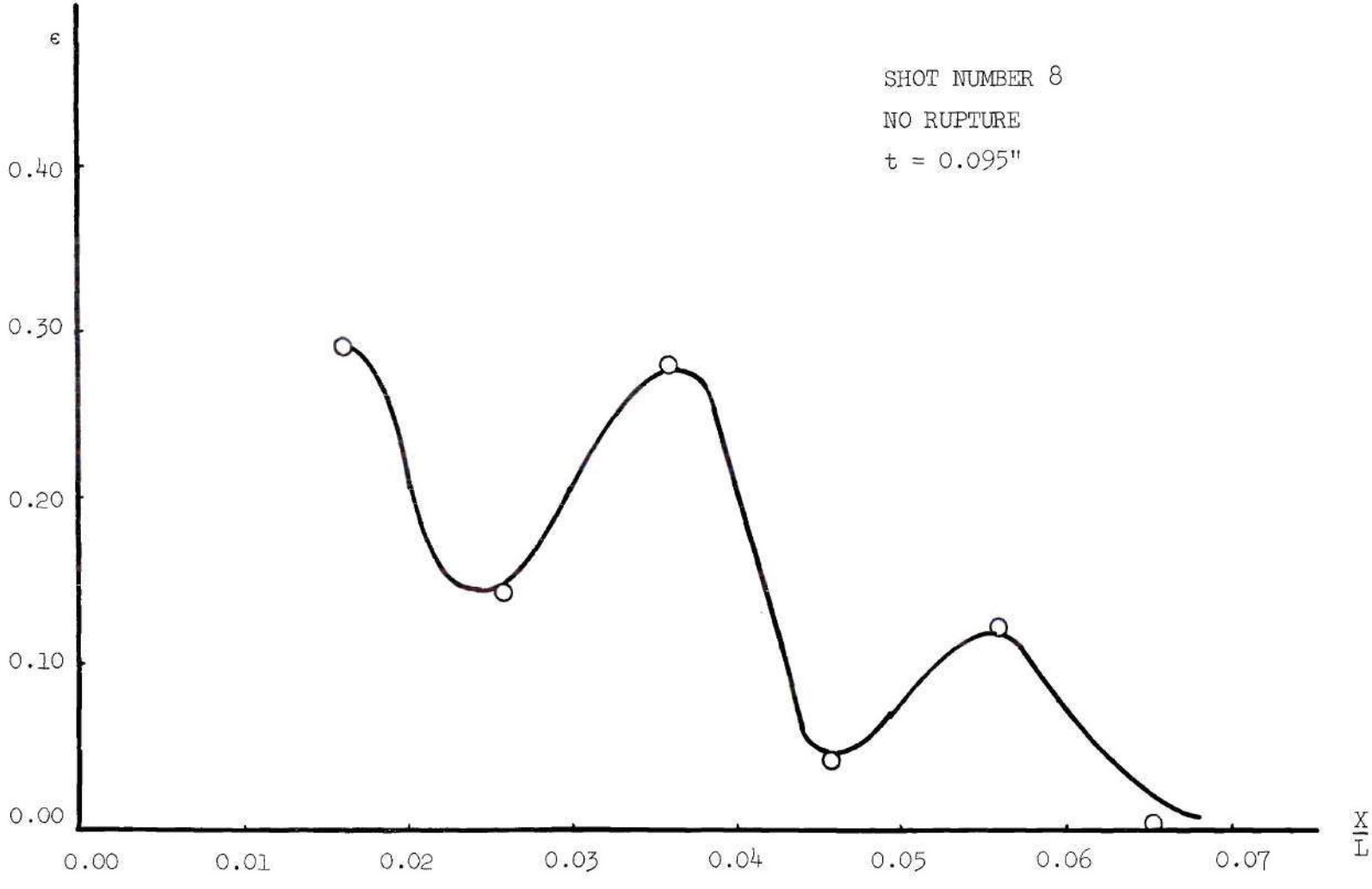

Figure 17. Strain Versus Nondimensional Length.

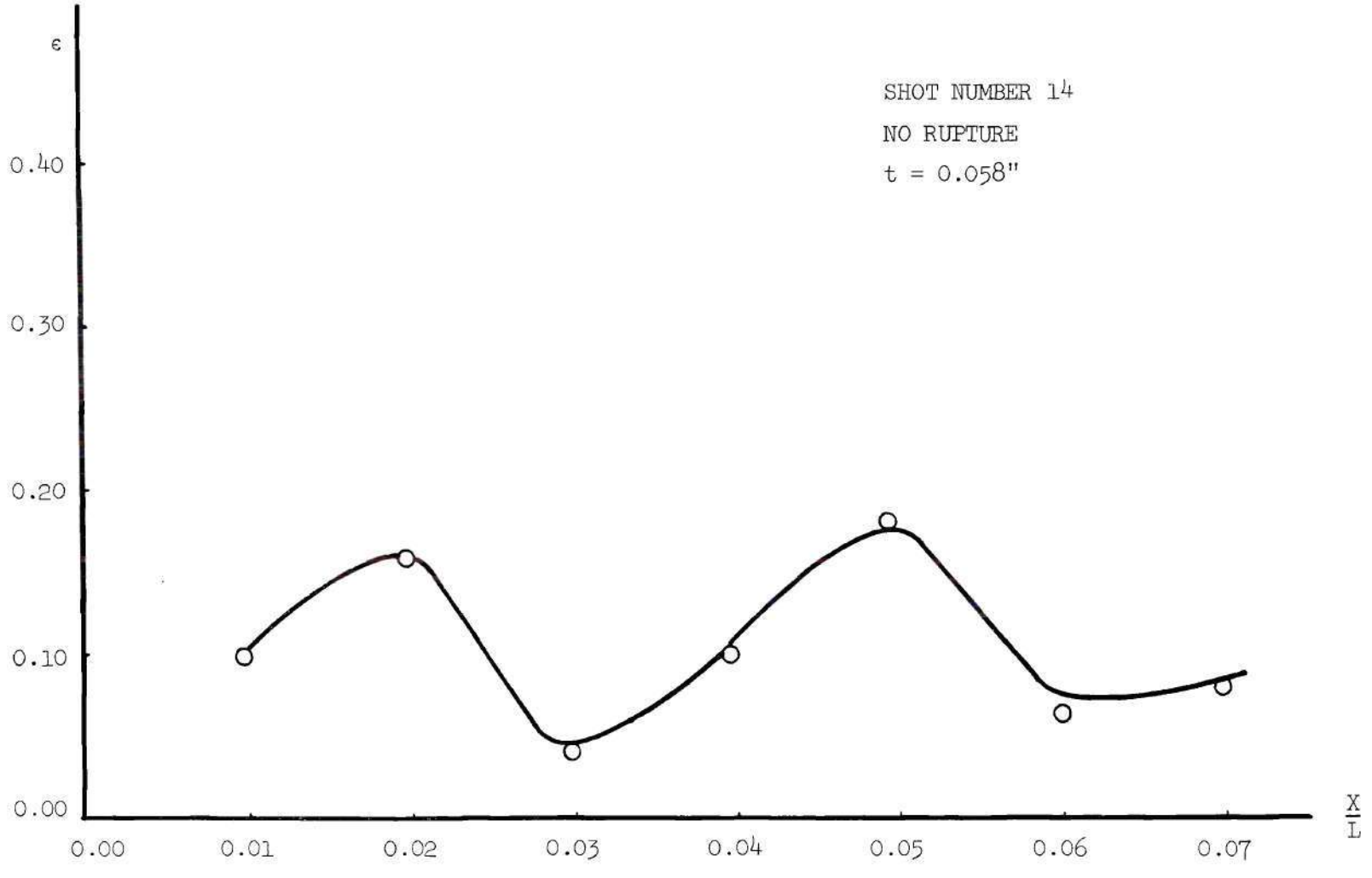

Figure 18. Strain Versus Nondimensional Length.

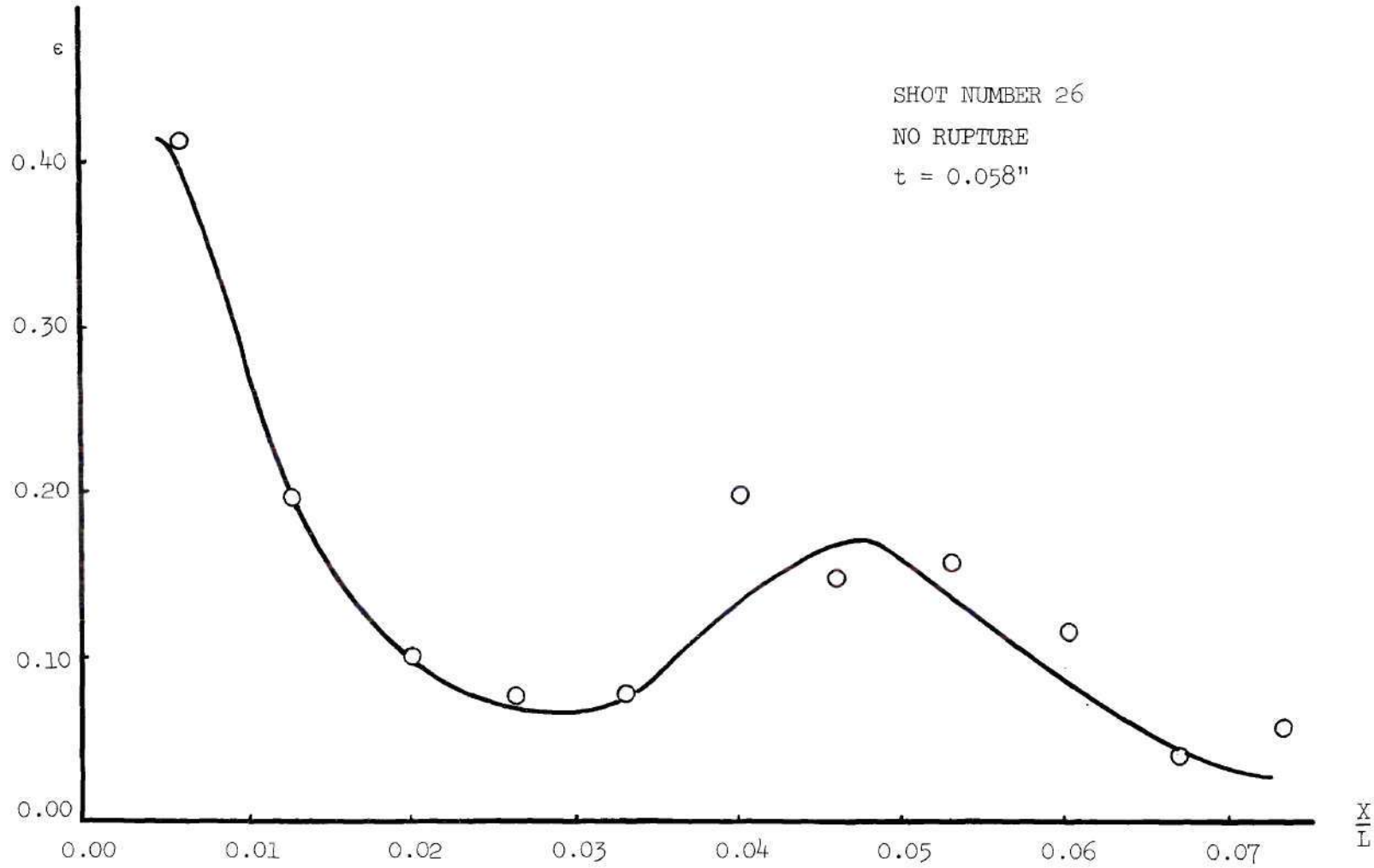

Figure 19. Strain Versus Nondimensional Length.

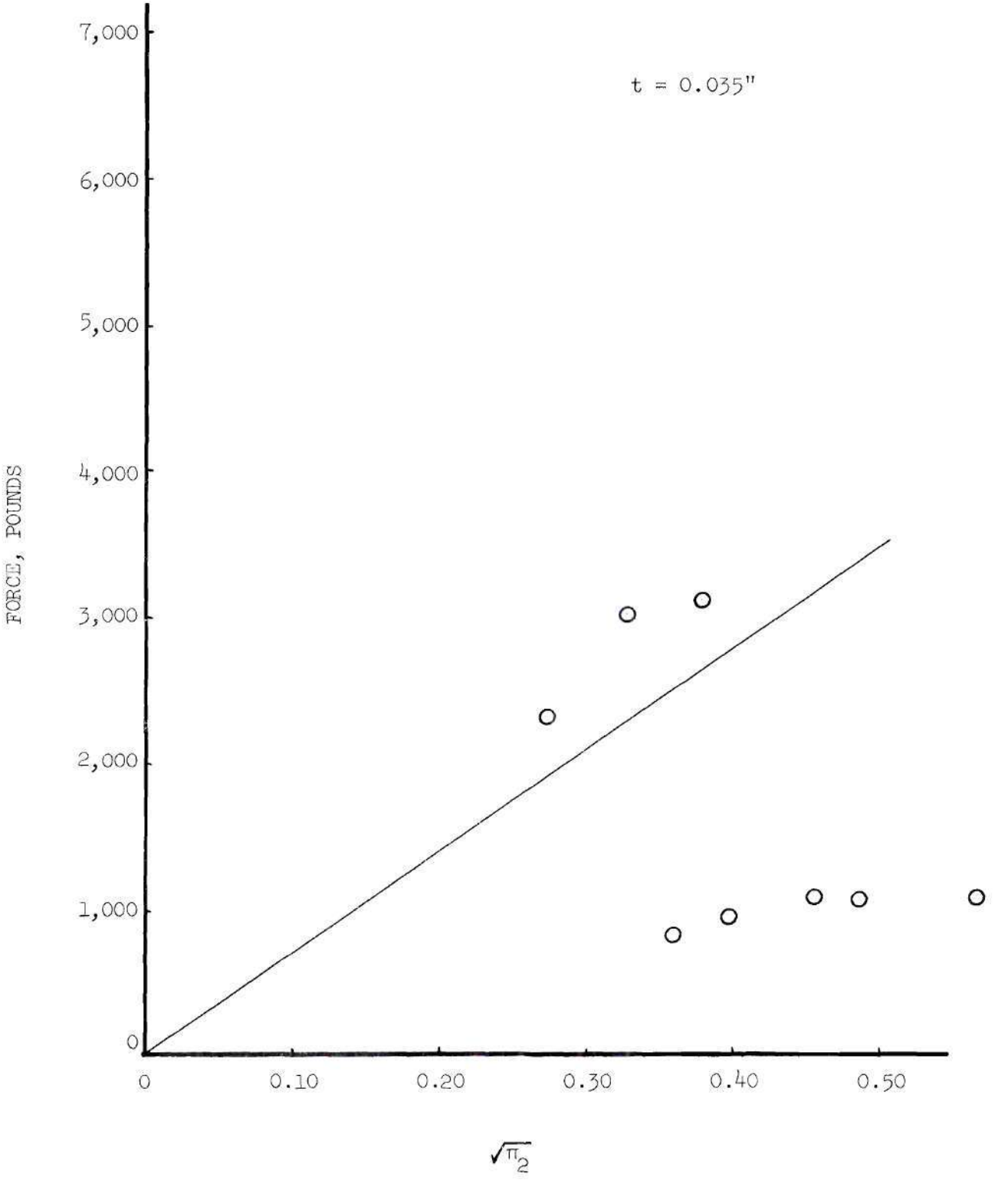

Figure 20. Force Versus Nondimensional Velocity

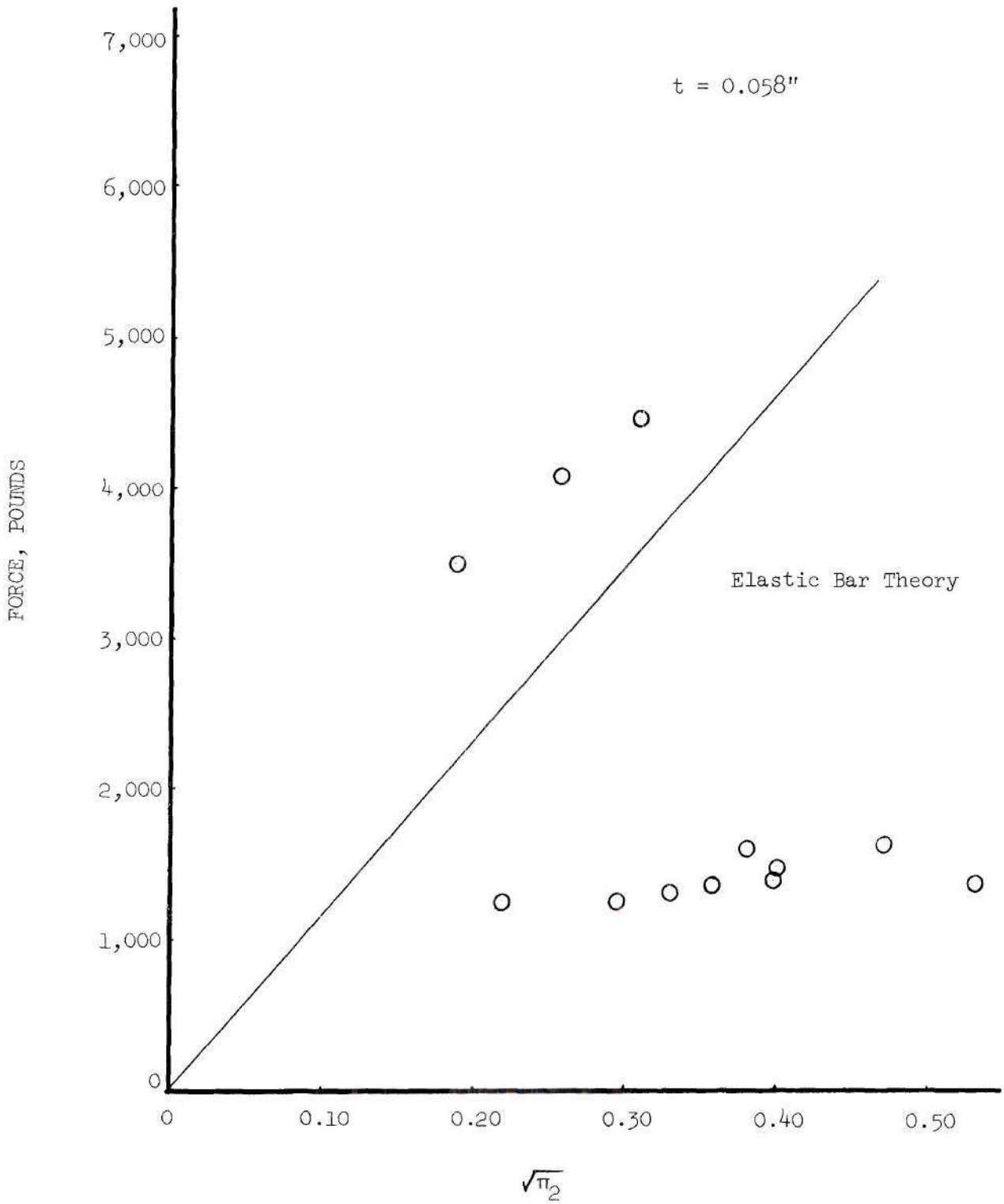

Figure 21. Force Versus Nondimensional Velocity

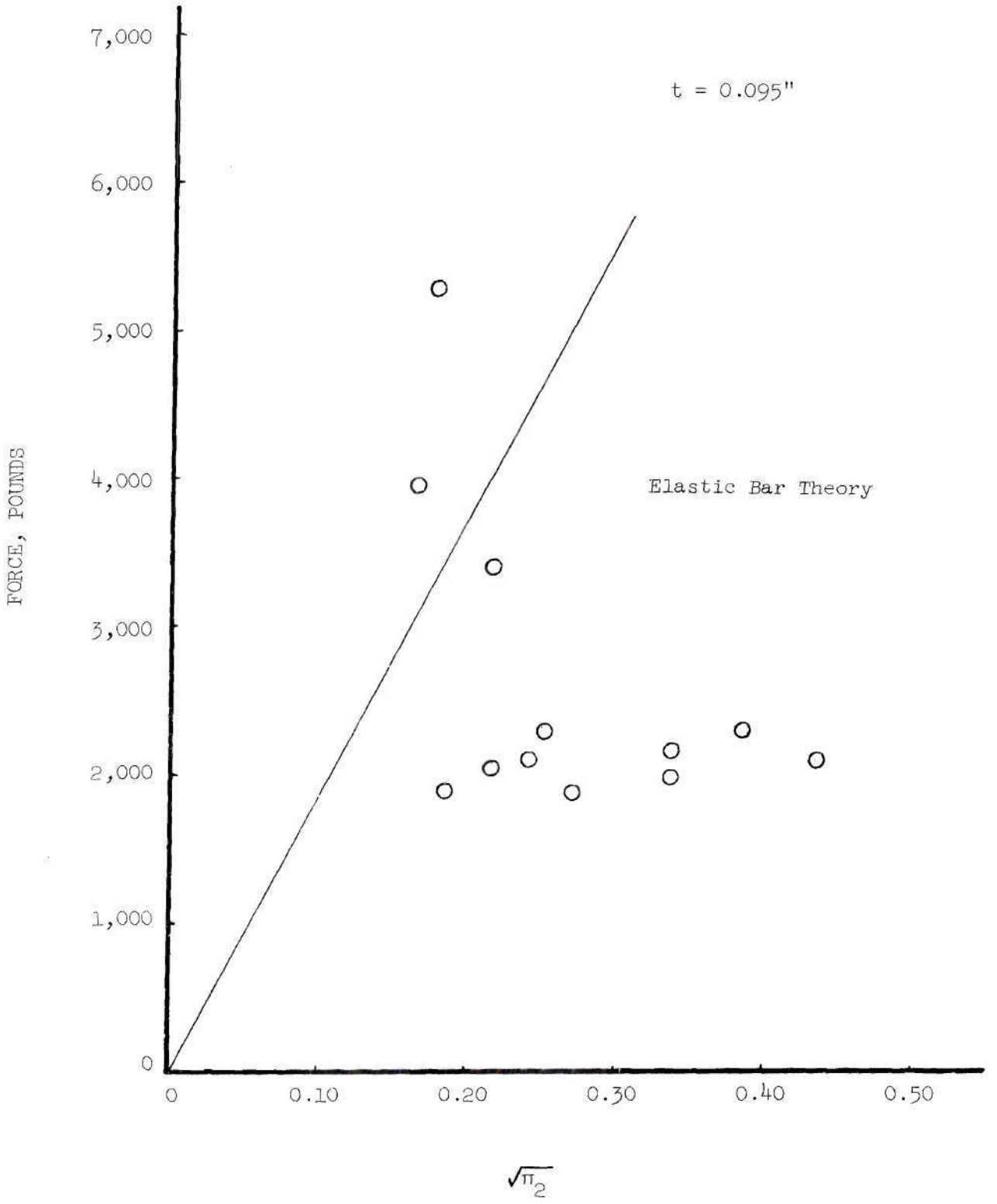

Figure 22. Force Versus Nondimensional Velocity

Table 1. Summation of Computer Print-Out

$\sqrt{\pi_2}$ Values

Observed	Calculated	Difference
.36050000	.37495520	-.01445520
.48062500	.48074100	-.00011600
.60127200	.58670070	.01457130
.29207900	.26857290	.02350610
.40481100	.42837500	-.02356400
.34844500	.34838690	.00005810
.28285500	.29190570	-.00905070
.37714045	.36814750	.00899295
.32999787	.32993970	.00005817

Sum of Squares = .0016918826

B(1) = .0000495171
B(2) = .63541569
B(3) = 49.286691
B(4) = .10947561
B(5) = -12.969777
B(6) = 1.2971799

Standard Deviation = .10023943
Standard Error = .02374786
R Square = .97895240

Table 2. Failure Velocities for the Cylinders Tested as Calculated from Equation 22.

Failure Velocity of AISI4130 Cylinders		
Thickness (in)	Length (in)	Failure Velocity (ft/sec)
.035	2.0	572.5
.035	2.5	520.9
.035	3.0	469.3
.035	3.5	417.8
.035	4.0	366.2
.058	2.0	417.8
.058	2.5	378.9
.058	3.0	339.9
.058	3.5	301.0
.058	4.0	262.1
.095	2.0	359.2
.095	2.5	340.6
.095	3.0	321.9
.095	3.5	303.3
.095	4.0	284.7

Table 3. Summary of Experimental Results

Shot	Velocity	Pressure	Duration	Length	Thick	Mass	PI2	PI3	PI4	Fail
1	295.8	.00	.0000, 00	2.000	.035	.052	.9193,-01	2.66	.046	No
2	253.1	.00	.0000, 00	3.000	.035	.079	.6731,-01	4.00	.046	No
3	222.2	.00	.0000, 00	4.000	.035	.105	.5186,-01	5.33	.046	No
4	243.3	.00	.0000, 00	2.000	.058	.079	.6217,-01	2.66	.077	No
5	238.6	.00	.0000, 00	2.000	.058	.079	.5982,-01	2.66	.077	No
6	197.2	.00	.0000, 00	3.000	.058	.119	.4085,-01	4.00	.077	No
7	184.8	-6797.07	.1000,-03	4.000	.058	.158	.3588,-01	5.33	.077	No
8	206.6	-6797.07	.8000,-04	2.000	.095	.114	.4483,-01	2.66	.126	No
9	168.0	-10603.43	.8000,-04	3.000	.095	.171	.2966,-01	4.00	.126	No
10	154.5	-7884.60	.1200,-03	4.000	.095	.202	.2509,-01	5.33	.126	No
11	366.3	-6253.30	.8000,-04	2.000	.035	.065	.1409, 00	2.66	.046	No
12	314.4	-5981.42	.1100,-03	3.000	.035	.083	.1038, 00	4.00	.046	No
13	261.7	-4622.01	.1500,-03	4.000	.035	.105	.7197,-01	5.33	.046	No
14	303.0	-8972.13	.6000,-04	2.000	.058	.088	.9644,-01	2.66	.077	No
15	251.2	-8156.48	.8000,-04	3.000	.058	.119	.6630,-01	4.00	.077	No
16	213.6	-2446.94	.8000,-04	4.000	.058	.154	.4795,-01	5.33	.077	No
17	241.5	-4622.01	.6000,-04	2.000	.095	.125	.6127,-01	2.66	.126	No
18	204.4	-4078.24	.9000,-04	3.000	.095	.180	.4392,-01	4.00	.126	No

(Continued)

Table 3 (Continued)

Shot	Velocity	Pressure	Duration	Length	Thick	Mass	PI2	PI3	PI4	Fail
20	176.9	-3806.36	.1000,-03	4.000	.095	.229	.3290,-01	5.33	.126	No
21	442.4	-2175.06	.8000,-04	2.000	.035	.063	.2056, 00	2.66	.046	No
22	381.6	-1903.18	.1100,-03	3.000	.035	.088	.1530, 00	4.00	.046	No
23	346.0	-1631.29	.1300,-03	4.000	.035	.105	.1257, 00	5.33	.046	No
24	352.1	.00	.0000, 00	4.000	.035	.101	.1302, 00	5.33	.046	No
25	387.5	.00	.0000, 00	2.000	.058	.083	.1577, 00	2.66	.077	No
26	322.5	-2582.88	.1000,-03	3.000	.058	.119	.1092, 00	4.00	.077	No
27	286.5	-2446.94	.9000,-04	4.000	.058	.154	.8623,-01	5.33	.077	No
28	316.4	.00	.0000, 00	2.000	.095	.119	.1051, 00	2.66	.126	No
29	259.0	-3806.36	.7000,-04	3.000	.095	.174	.7049,-01	4.00	.126	No
30	233.1	-4214.18	.1000,-03	4.000	.095	.224	.5706,-01	5.33	.126	No
33	549.4	-2175.06	.1200,-03	2.000	.035	.046	.3170, 00	2.66	.046	No
34	469.4	-2039.12	.1300,-03	3.000	.035	.088	.2315, 00	4.00	.046	No
35	413.2	.00	.0000, 00	4.000	.035	.103	.1793, 00	5.33	.046	Yes
36	465.1	-3262.59	.7000,-04	2.000	.058	.090	.2272, 00	2.66	.077	Yes
37	378.7	-2718.82	.8000,-04	3.000	.058	.123	.1506, 00	4.00	.077	No
38	348.4	-2718.82	.1100,-03	4.000	.058	.156	.1275, 00	5.33	.077	Yes
39	370.3	-4622.01	.7000,-04	2.000	.095	.125	.1440, 00	2.66	.126	No

(Continued)

Table 3 (Concluded)

Shot	Velocity	Pressure	Duration	Length	Thick	Mass	PI2	PI3	PI4	Fail
40	321.5	-3942.30	.1300,-03	3.000	.095	.174	.1085, 00	4.00	.126	No
44	321.5	-4350.12	.1100,-03	4.000	.095	.218	.1085, 00	5.33	.126	No
45	369.0	.00	.0000, 00	3.000	.095	.154	.1430, 00	4.00	.126	Yes
46	420.1	-4214.18	.8000,-04	2.000	.095	.121	.1854, 00	2.66	.126	Yes
49	390.6	-2990.71	.0000, 00	4.000	.058	.154	.1602, 00	5.33	.077	Yes
50	446.4	.00	.0000, 00	3.000	.058	.116	.2093, 00	4.00	.077	Yes
51	520.8	-2718.82	.1200,-03	3.000	.058	.088	.2849, 00	4.00	.077	Yes
52	537.6	.00	.0000, 00	3.000	.035	.083	.3035, 00	4.00	.046	No
53	471.6	.00	.0000, 00	4.000	.035	.105	.207	5.33	.046	No

Velocity in feet per second
Pressure in pounds per square inch
Duration in seconds
Length in inches
Thickness in inches
Mass in grams
All others dimensionless

CHAPTER V

CONCLUSIONS

Although equation (22) is empirical, it can be said to be a usable and reasonably accurate equation for cylinder failure in the sense defined in Chapter I. Although these values are considerably higher than extrapolated from the equation given by Young, Stoneking, and Colp (32) for close cylinders, it should be noted that the present study is based on a different failure criterion, a different thickness range, and a complete dimensional analysis. The low standard deviation and standard error in Table 1 show that the curve fits the experimental data well, while the value of the correlation coefficient ("R square") close to 1.00 shows that the curve was of the correct type and contained enough terms to fit the data points well. Some observed and calculated values for $\sqrt{\pi_2}$ are given for reference.

Most of the cylinders failed by shearing out a ring, as shown in Fig. 28. This is essentially the same type failure as obtained in (32). Thus, apparently if an end cap is designed with sufficient strength and is welded onto the shell correctly, the failure mode of open and closed-end cylinders will correspond.

The graphs concerned with buckling phenomena show considerable scatter. However, the scatter is not any worse than that usually found in static compression tests of similar structures (33), and is probably caused mainly by structural imperfections and variations in the planeness

of impacts.

Although the evidence is still insufficient, it might be hypothesized on the basis of the experiments that impact force increases in direct proportion to impact velocity, until some point which by analogy might be called the "impact buckling point" is reached, after which the force decreases exponentially with the velocity. It should be noted that the accuracy of the force measuring instrumentation is somewhat limited, and very short duration force pulses cannot be detected or measured.

The strain-length plots are subject to much speculation. Some of the measurements could easily be incorrect. The best that can be said is that they agree qualitatively with the plots given in (32), and with some preliminary theoretical results obtained at Georgia Tech using membrane theory.

The experimental setup as used provides an effective and relatively easy method of gathering impact data. In particular, the photogrid method, if carefully used, is an easy and straightforward, if tedious, method of measuring plastic strains.

CHAPTER VI

RECOMMENDATIONS

Experimental

The scope of the experimental program here is obviously too small to provide a complete solution to the problem of impact of cylinders. With this in mind, the following additional research is recommended:

a. The number of samples tested should be increased considerably so the failures can be judged on a statistical basis, and errors can be estimated.

b. The program should be extended to include several more materials, so that the effects of material properties can be judged.

c. The photogrid process, although essentially perfected in the form used here, can use some additional refinements. Finer and sharper grids can be achieved by more careful application of the light sensitive coating. The master negative used should be thinner, and the ratio of grid line thickness to grid to square thickness should be decreased considerably. A jig should be constructed to align the negative correctly with the shell. The surface on which the grid is to be coated should be smooth, and an accurate method of aligning the measuring microscope is needed.

d. The movies, although useful for qualitative data taking, are not usable for quantitative data taking. A camera with a speed of approximately 50,000 frames per second and a negative size

similar to the 35mm Fastax is needed. It would then be possible to use the motion picture frames, in conjunction with the photogrids, to measure dynamic buckling characteristics and plastic wave propagation.

Theoretical

On the basis of observations of the failure modes of open and closed end cylinders, it can be concluded that the frictional force created by the impact of one smooth solid upon another is so high that a "fixed end" boundary condition is created, even in an open ended cylinder. Thus, the interest in the case of an open ended cylinder has no connection with physical reality. It would seem advantageous to do all mathematical analysis for the case of a closed end cylinder, and verify these analyses experimentally with open ended cylinders, thus, saving the cost and trouble of welding.

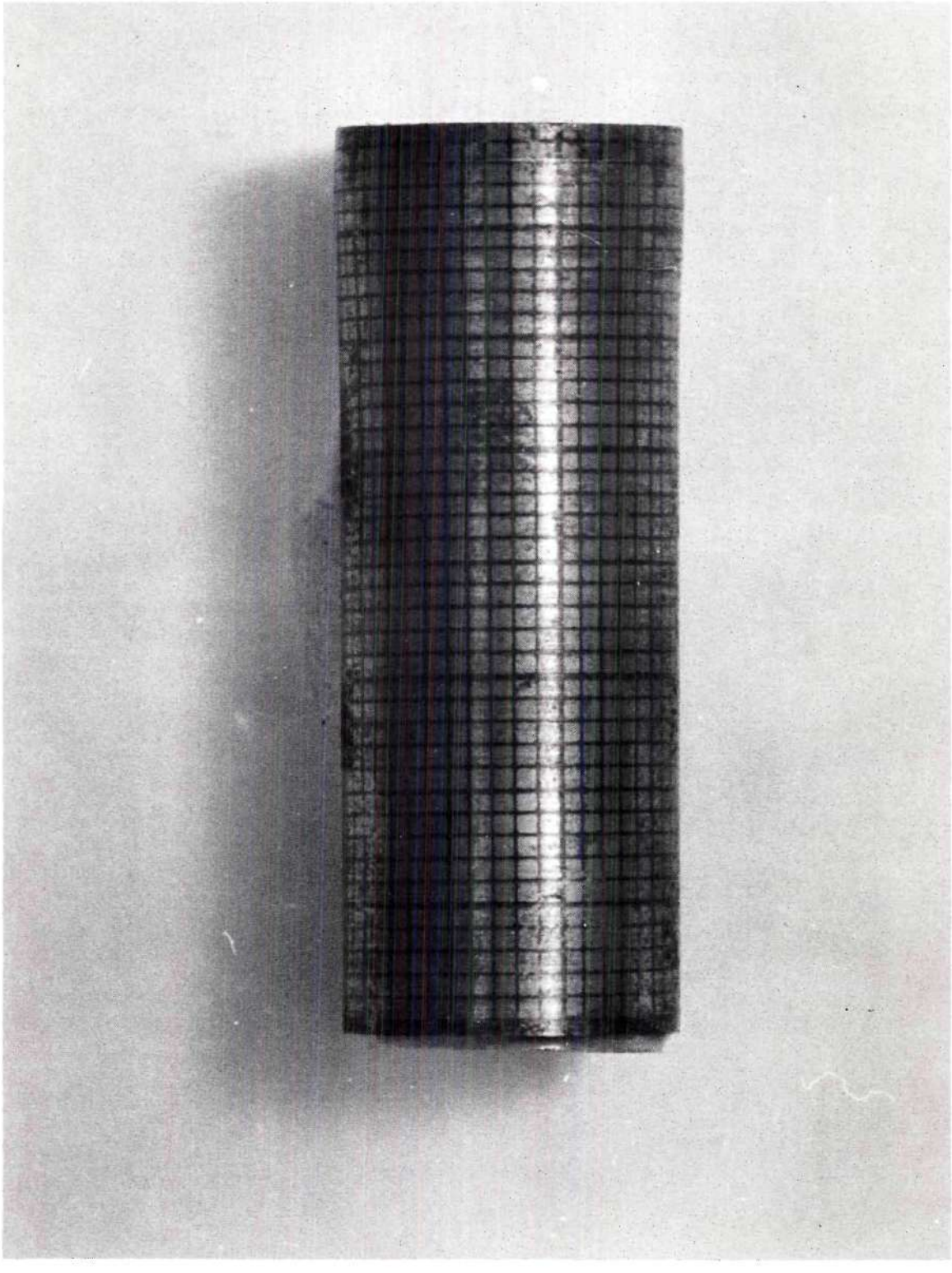

Figure 23. A Typical Cylinder Before Impact.

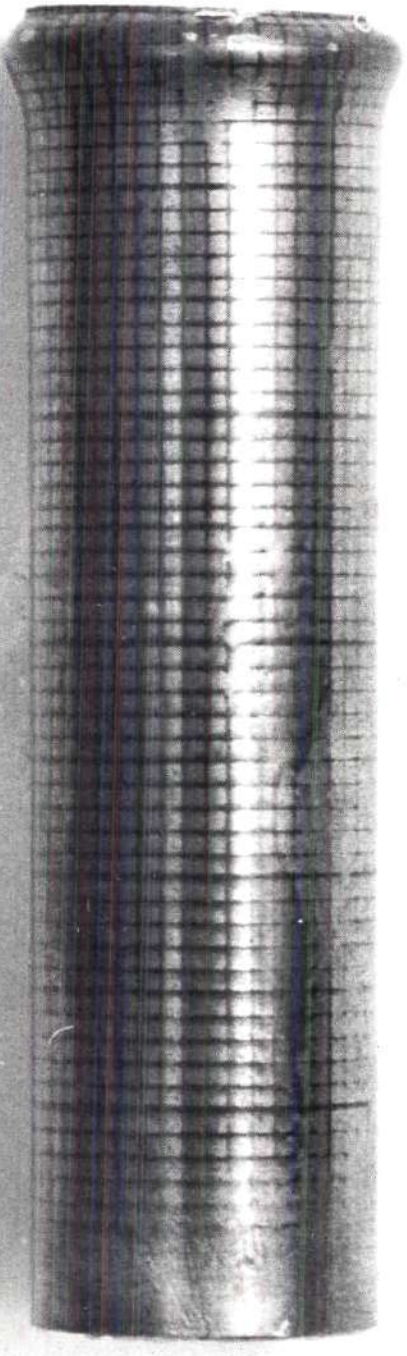

Figure 24. Shot Number 12 After Impact.

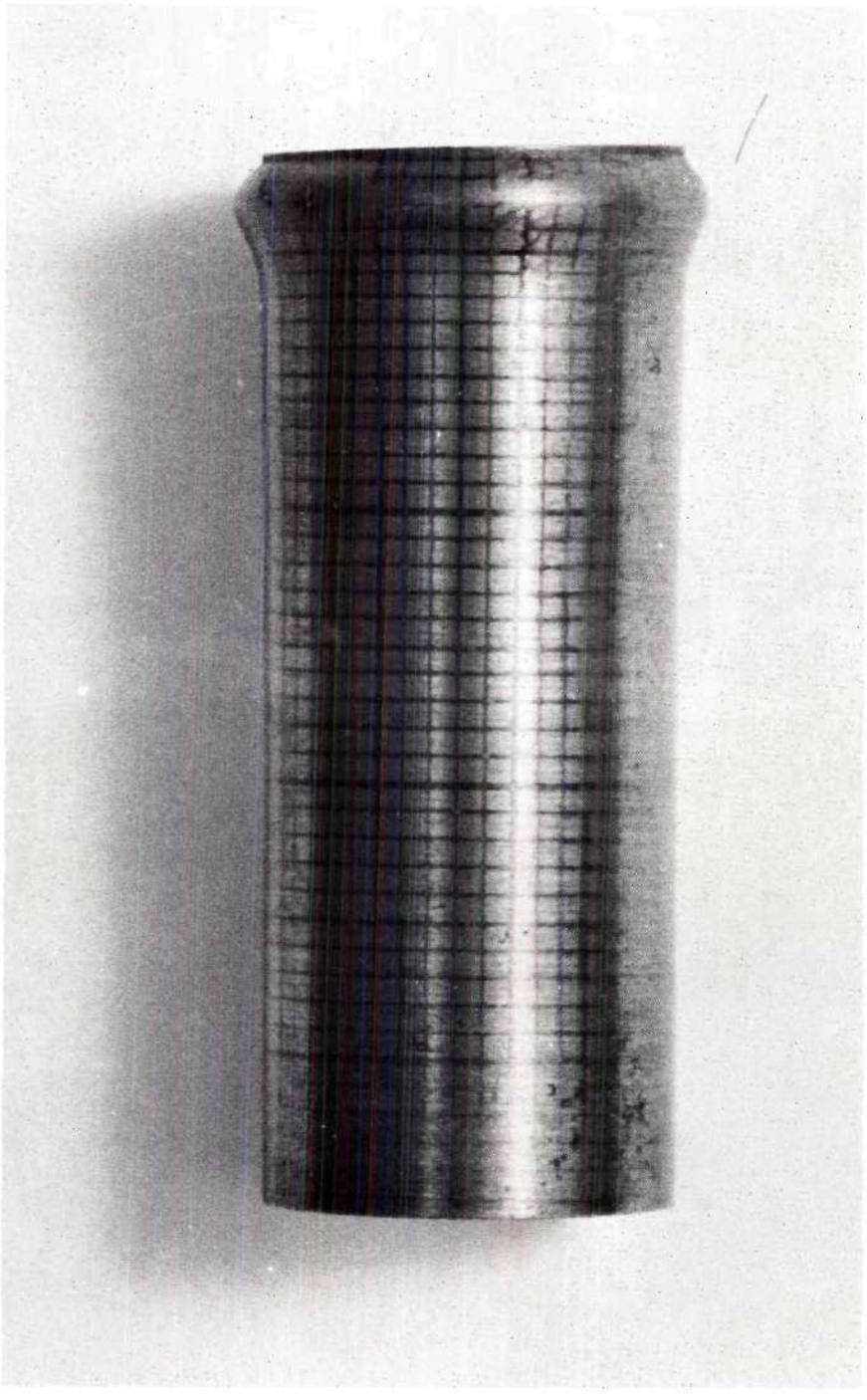

Figure 25. Shot Number 11 After Impact.

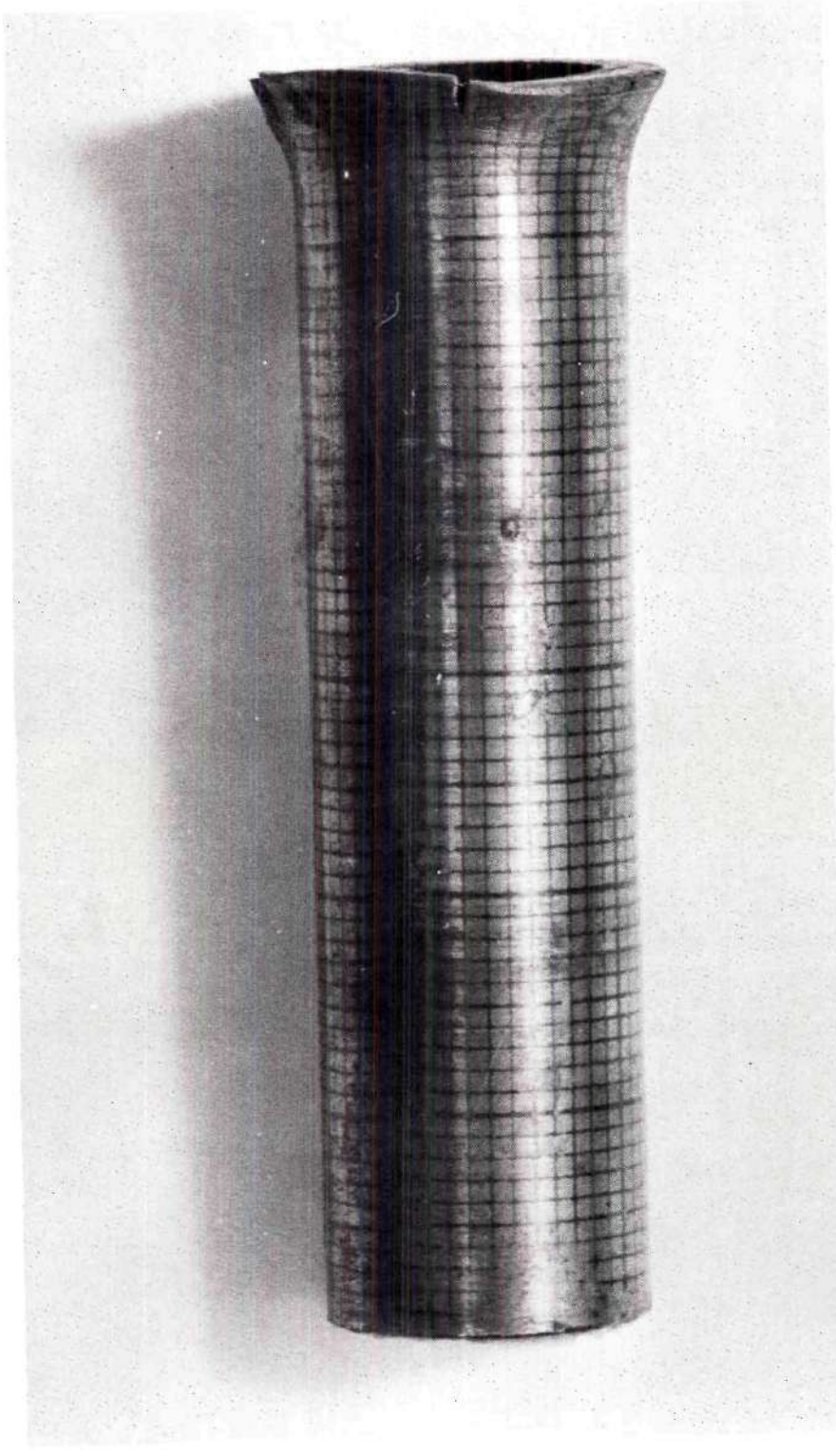

Figure 26. Shot Number 45 After Impact.

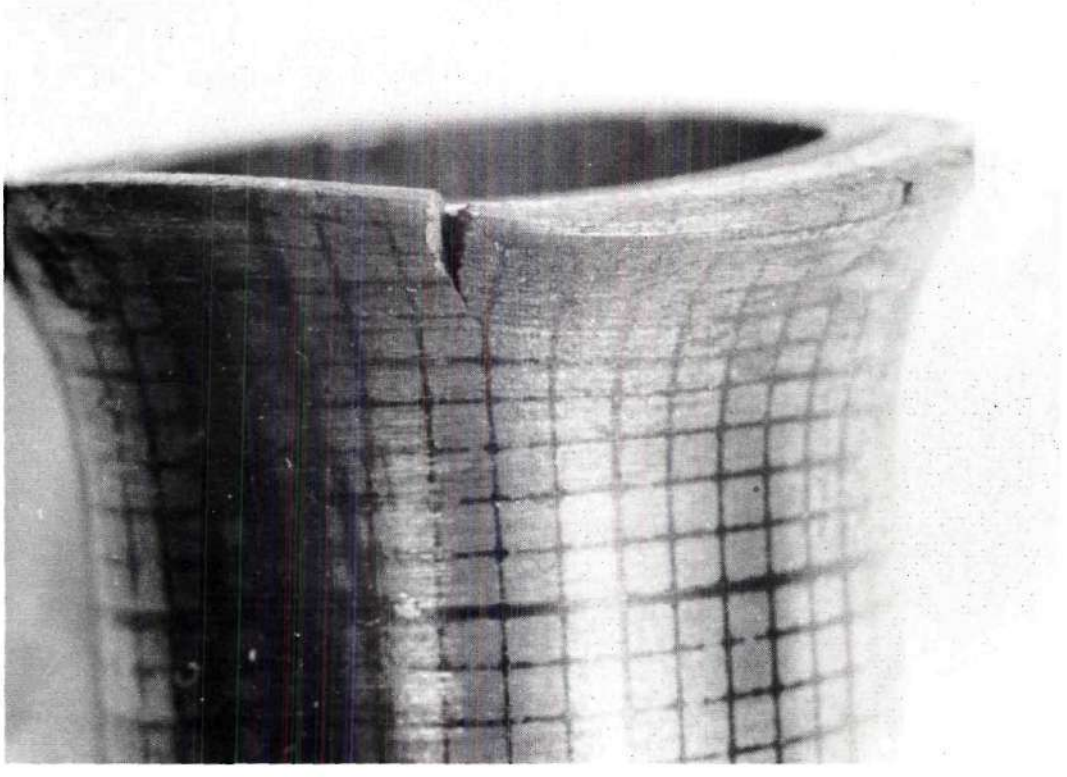

Figure 27. A Close-up Illustration of a Failed Area On Shot Number 45.

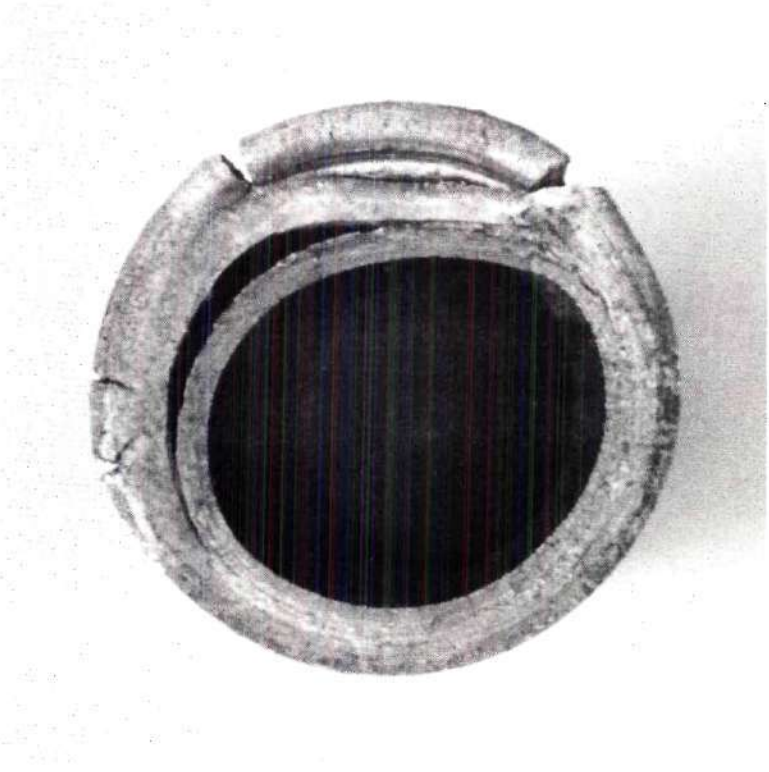

Figure 28. The Impact End of Shot Number 45.

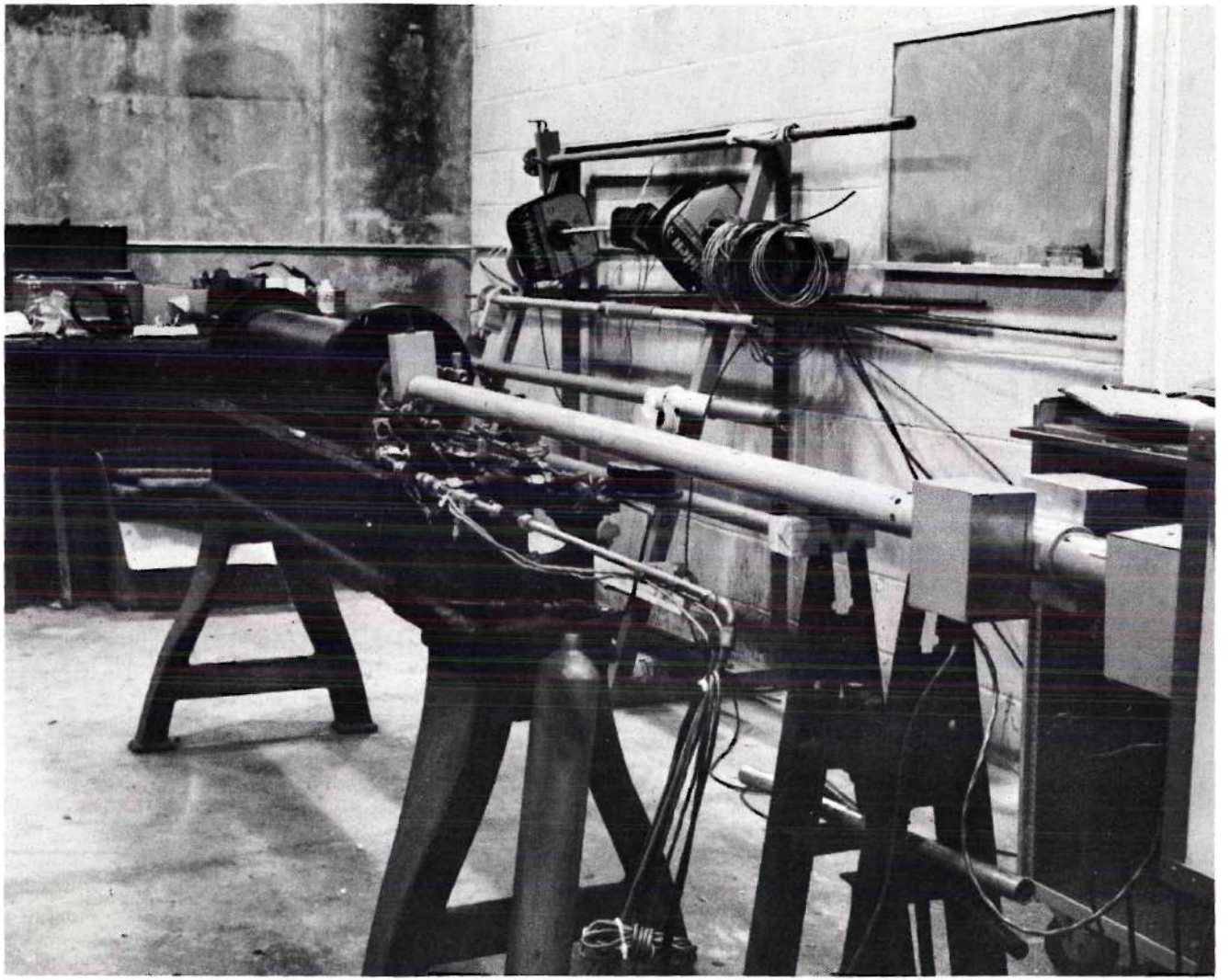

Figure 29. The Air Gun.

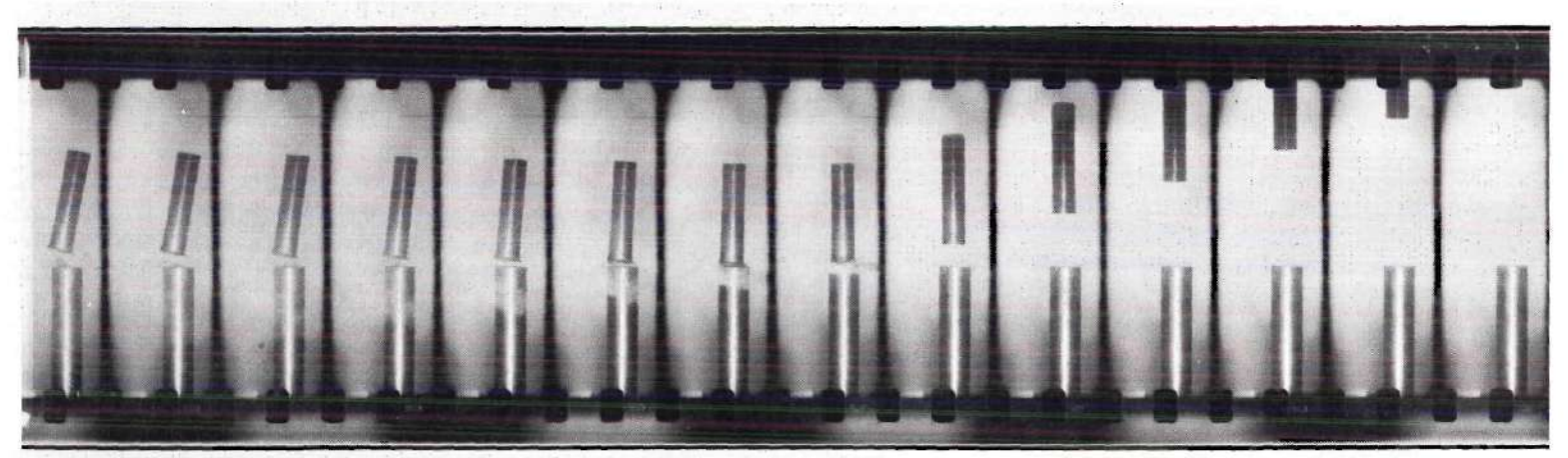

Figure 30. Motion Picture of an Impact.

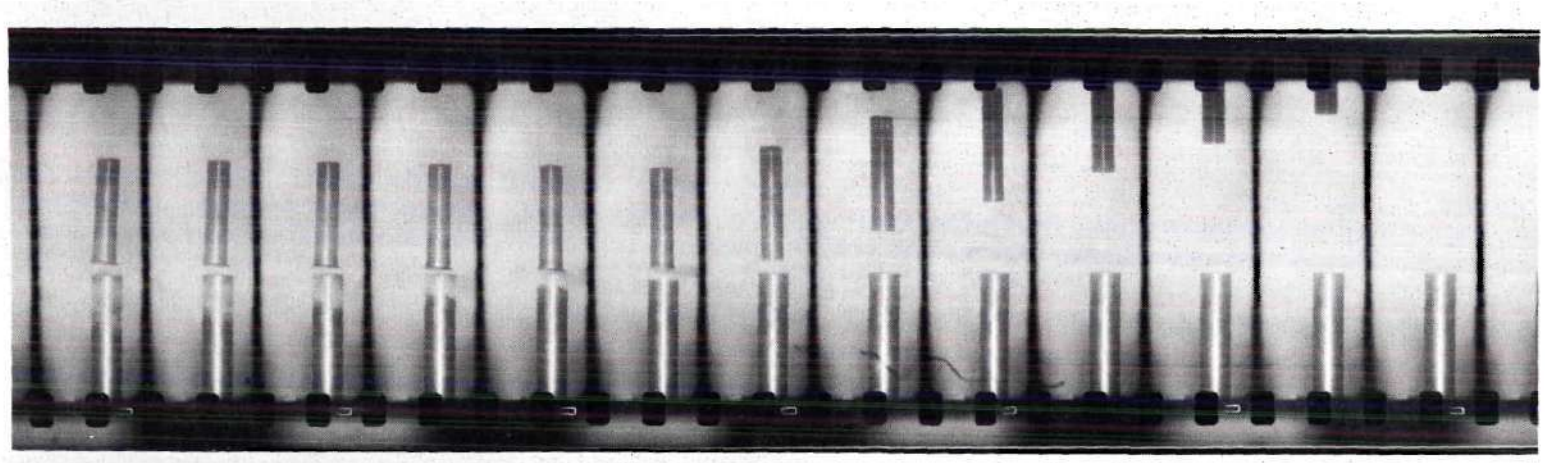

Figure 31. Motion Picture of an Impact.

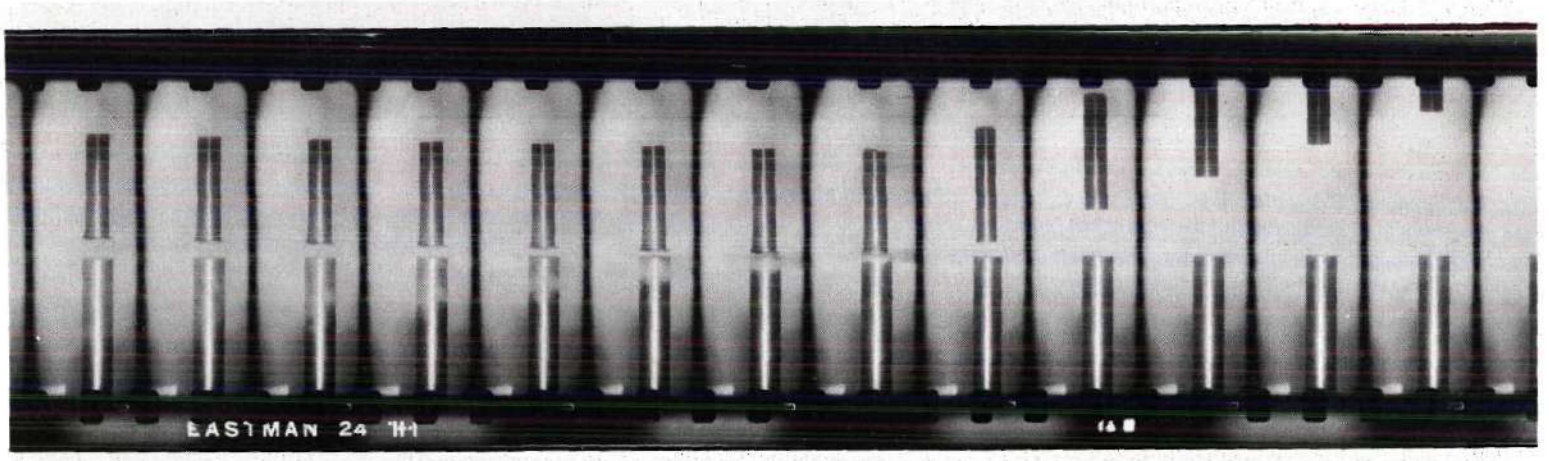

Figure 32. Motion Picture of an Impact.

Table 4. Data Sheet for Shot 18

PROJECT A-743

PLASTIC STRAINS IN CYLINDRICAL SHELLS DATA SHEET

SHOT NO. 18

DIAMETER = 3/4 inch

LENGTH = 3 inches

THICKNESS = 0.095 inches

MASS = 0.154 grams

Velocity = 204.4 fps

Estimated distance from impact end to station 1 = 0.5 square.

1 square = 1/50 inch

L_x measured in thousandths of an inch

STATION	L_x
1	44
2	49
3	49
4	48
5	49
6	48
7	46
8	49
9	51

Table 5. Data Sheet for Shot 45

PROJECT A-743

PLASTIC STRAINS IN CYLINDRICAL SHEELS DATA SHEET

SHOT NO. 45

DIAMETER = 3/4 inch

LENGTH = 3 inches

THICKNESS = 0.095 inches

MASS = 0.154 grams

Velocity = 369.0 fps

Estimated distance from impact end to station 1 = 0.5 square.

1 square = 1/50 inch

L_x measured in thousandths of an inch

STATION	L_x
1	--
2	41
3	40
4	40
5	38
6	45
7	42
8	49
9	46
10	49
11	45
12	48
13	48

(Continued)

Table 5 (Concluded)

STATION	L_x
14	48
15	45
16	48
17	47
18	49
19	50
20	48
21	50
22	50

APPENDIX

DESIGN OF CYLINDRICAL SHELLS TO WITHSTAND IMPACT LOADS

Figure 4 provides a method of designing cylindrical shells to withstand axial impact conditions. It is used in the following manner: First, the length and diameter of the cylinder are chosen by consideration of the required volume and geometry. This determines $\frac{L}{D}$, which is read as π_3 on the horizontal axis. Then, the required failure velocity is determined and is read on the vertical axis. The point at which these two values intersect is plotted, and then the $\frac{t}{D}$ ratio necessary is that closest to and above the intersection.

As an example, suppose a shell 1.0 inch diameter and 2.5 cubic inch volume is required to withstand an impact velocity of 500 fps Since $V = \frac{\pi}{4} D^2 L$, it is seen that:

$$L = \frac{4}{\pi} \frac{V}{D^2} = \frac{4}{\pi} V = \frac{4}{\pi} (2.5) = 3.18 \text{ in.}$$

Thus, $\frac{L}{D} = \frac{3.18}{1.00} = 3.18$. Now, reading 3.18 on the horizontal axis and 500 fps on the vertical axis, the $\frac{t}{D}$ ratio directly above the point is $\frac{t}{D} = 0.045$. Thus, the required thickness is 0.045 inch.

LITERATURE CITED

1. Newton, I., Philosophiae Naturalis Principia Mathematica. (1686) (Translated into English by A. Motte). New York, D. Adee, 1848.

2. St. Venant, B.d., and Flamant, "Courses Représentatives des Lois Du Choc Longitudinal Et Du Choc Transversal D'une Barre Prismatique," J. École Polytechnique, Paris, 59, 1889, 97.

3. Boussinesq. J., Applications Des Potentials A L' Étude de l'Equilibre Et Du Mouvement Des Solides Elastiques. Paris Gauthier-Villars, 1885.

4. Von Karman, T., On the Propagation of Plastic Deformation in Solids, NDRC Report No. A-29, February 2, 1942. (This Report was classified and not available to the public until after World War II.)

5. Von Karman, T., and P. E. Duwez, "On the Propagation of Plastic Strains in Solids," presented at the Sixth International Conference for Applied Mechanics, September, 1946, Paris.

6. Clark, D. S., and P. E. Duwez, "The Influence of Strain Rate On Some Tensile Properties of Steel," Proceedsings, A.S.T.M., 1950.

7. Parker, E. R., and C Ferguson, "The Effect of Strain Rate Upon the Tensile Impact Strength of Some Metals," Transactions, Am. Soc. Metals, Vol. 30, p. 68 (1942).

8. Malvern, L. E., "The Propagation of Longitudinal Waves of Plastic Deformation in a Bar of Material Exhibiting a Strain Rate Effect," Journal of Applied Mechanics, June 1951.

9. Hodge, P. G., "Impact Pressure Loading of Rigid-Plastic Cylindrical Shells," J. Mech. and Phys. Solids, 1955.

10. Lin, T. C., and G. W. Morgan, "A Study of the Axisymmetric Vibrations of Cylindrical Shells as Affected by Rotary Inertia and Transverse Shear," Journal of Applied Mechanics, June, 1956.

11. Timoshenko, S. P., "On the Correction for Shear of the Differential Equation for Transverse Vibrations of Prismatic Bars," Philosophical Magazine, Series 6, Vol. 41, 1921.

12. Hermann, G., and I. Mirsky, "Three-Dimensional and Shell-Theory Analysis of Axially Symmetric Motions of Cylinders," Journal of Applied Mechanics, December, 1956.

13. Mirsky, I., and G. Herrmann, "Axially Symmetric Motions of Thick Cylindrical Shells," Journal of Applied Mechanics, March, 1958.

14. Mirsky, I., "Vibrations of Orthotropic, Thick, Cylindrical Shells," The Journal of the Acoustical Society of America, Vol. 36, No. 1, January, 1964.

15. Berkowitz, H. M., "Longitudinal Impact of a Semi-infinite Elastic Cylindrical Shell," Journal of Applied Mechanics, September, 1963.

16. Spillers, W. R., "Wave Propagation in a Thin Cylindrical Shell," Journal of Applied Mechanics, June, 1965.

17 Buckingham, E., "On Physically Similar Systems; Illustrations of the Use of Dimensional Equations," Physical Review, Second Series, Vol. IV, No. 4, 1914.

18. Buckingham, E., "Model Experiments and the Forms of Empirical Equations," Transactions, A.S.M.E., Paper No. 1487, 1915.

19. Langhaar, H. L., "A Summary of Dimensional Analysis," Journal of the Franklin Institute, Vol. 242, No. 6, December, 1942.

20. Ripperger, E. A., "Stress-Strain Characteristics of Materials at High Strain Rates, Part V, Dynamic Compressive Yield Stresses," University of Texas, Structural Mechanics Research Laboratory, August, 1960.

21. Karnes, C. H., "Stress-Strain Characteristics of Materials at High Strain Rates, Part IV, Experimental and Theoretical Analysis of Plastic Impacts on Short Cylinders," University of Texas, Structural Mechanics Research Laboratory, August, 1960.

22. Benedick, W. B., Tech, Mem. 79-56-51, Sandia Corporation.

23. Hopkinson, B., "A Method of Measuring the Pressure Produced in the Detonation of High Explosives or by the Impact of Bullets," Phil. Trans. Roy. Soc., 213, Sec. A, 1914.

24. Davies, R. M., "A Critical Study of the Hopkinson Pressure Bars," Phil. Trans. Roy. Soc., 240, Sec. A, 1948.

25. Ripperger, E. A., "The Response of Pulses in Cylindrical Bars," Contract N6-ONR-251, T. O. 12(Nr-064-241).

26. Nisbet, J. I., J. N. Brennan, and H. I. Tapley, "High Frequency Strain Gage and Accelerometer Calibration," Journal of the Acoustical Society of America, 32, No. 1.

27. Durelli, Phillips, and Tsao, Analysis of Stress and Strain, McGraw-Hill, New York, 1958.

28. Templin, R. L., "Ductility Testing of Aluminum and Aluminum Alloy Sheet," Proceedings, A.S.T.M., Vol. 36, 1936.

29. Brewer, G. A., and R. B. Glassco, "Determination of Strain Distribution by the Photogrid Process," J. Aero. Sci., Vol. 9, No. 1, November, 1941.

30. McLaren, D. D., "The Photo-Grid Process for Measuring Strains Caused by Underwater Explosions," Experimental Stress Analysis.

31. Miller, J. A., "Improved Photogrid Technique for the Determination of Strain Over Short Gage Lengths," Experimental Stress Analysis, 1952.

32. Young, C. W., C. E. Stoneking, and J. L. Colp, "Containment Capsule Impact Safety Study, Phase A, Progress Report," Sandia Corporation, SC-RR-65-9.

33. Timoshenko, Stephen P., and James M. Gere, Theory of Elastic Stability, McGraw-Hill, 1961.

34. Kolsky, H., Stress Waves in Solids, Dover Publications, 1963.

35. Goldsmith, Werner, Impact, Edward Arnold, 1960.